

## Phosphorylation of *Thellungiella salsuginea* Dehydrins TsDHN-1 and TsDHN-2 Facilitates Cation-Induced Conformational Changes and Actin Assembly

Luna N. Rahman,<sup>†</sup> Graham S. T. Smith,<sup>†</sup> Vladimir V. Bamm,<sup>†</sup> Janine A. M. Voyer-Grant,<sup>†</sup> Barbara A. Moffatt,<sup>‡</sup> John R. Dutcher,<sup>§</sup> and George Harauz\*,<sup>†</sup>

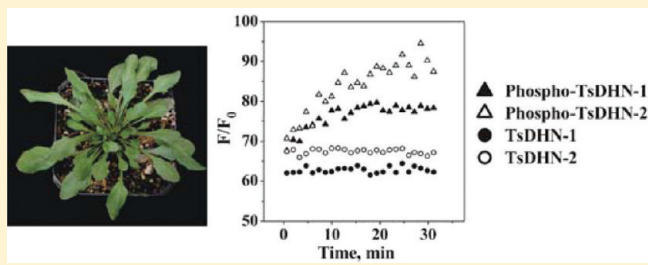
<sup>†</sup>Department of Molecular and Cellular Biology, University of Guelph, Guelph, ON N1G 2W1, Canada

<sup>‡</sup>Department of Biology, University of Waterloo, Waterloo, ON N2L 3G1, Canada

<sup>§</sup>Department of Physics, University of Guelph, Guelph, ON N1G 2W1, Canada

### Supporting Information

**ABSTRACT:** Group 2 late embryogenesis abundant (LEA) proteins, also known as dehydrins, are intrinsically disordered proteins that are expressed in plants experiencing extreme environmental conditions such as drought or low temperatures. These proteins are characterized by the presence of at least one conserved, lysine-rich K-segment and sometimes by one or more serine-rich S-segments that are phosphorylated. Dehydrins may stabilize proteins and membrane structures during environmental stress and can sequester and scavenge metal ions. Here, we investigate how the conformations of two dehydrins from *Thellungiella salsuginea*, denoted as TsDHN-1 (acidic) and TsDHN-2 (basic), are affected by pH, interactions with cations and membranes, and phosphorylation. Both TsDHN-1 and TsDHN-2 were expressed as SUMO fusion proteins for *in vitro* phosphorylation by casein kinase II (CKII), and structural analysis by circular dichroism and attenuated total reflection-Fourier transform infrared spectroscopy. We show that the polyproline II conformation can be induced in the dehydrins by their environmental conditions, including changes in the concentration of divalent cations such as  $\text{Ca}^{2+}$ . The assembly of actin by these dehydrins was assessed by sedimentation assays and viewed by transmission electron and atomic force microscopy. Phosphorylation allowed both dehydrins to polymerize actin filaments. These results support the hypothesis that dehydrins stabilize the cytoskeleton under stress conditions and further that phosphorylation may be an important feature of this stabilization.



Crop yields are severely affected by various environmental stresses such as low temperatures and drought. Low temperatures may lead to poor germination, stunted seedlings, yellowing of leaves (chlorosis), reduced leaf expansion and wilting, and eventual tissue necrosis. However, low-temperature-tolerant plants have evolved many ways of coping with environmental stresses. One response to these conditions is the induction of genes that encode the late embryogenesis abundant (LEA) proteins.<sup>1,2</sup> To date, the group 2 LEA proteins, also known as dehydrins, have been the most extensively investigated.<sup>3–6</sup> The way in which LEA proteins in general, and dehydrins in particular, function to protect plants from environmental stress is thought to involve diverse mechanisms as previously reviewed (e.g., refs 6–9). They are proposed to stabilize and maintain the integrity of intracellular enzymes,<sup>10–13</sup> plasma and organellar membranes,<sup>8,9,14,15</sup> actin microfilaments,<sup>16</sup> the extracellular matrix,<sup>17</sup> and nucleic acids.<sup>18</sup> Most LEA proteins are intrinsically disordered proteins (IDPs).<sup>12,19,20</sup> It is generally accepted that the intrinsically disordered and extended conformation of LEA proteins allows them to sequester water and sugars in a tightly hydrogen-

bonded network to form a hydrocolloid or gel.<sup>20,21</sup> They have also been proposed to sequester calcium and scavenge heavy metals such as  $\text{Zn}^{2+}$ ,  $\text{Cd}^{2+}$ , and  $\text{Cu}^{2+}$  and free radicals *in vivo*.<sup>22–29</sup> The association of metals with these other plant dehydrins has been shown to promote binding to DNA,<sup>18,26</sup> conformational changes,<sup>27</sup> heavy metal tolerance of the organism,<sup>28</sup> and reversible aggregation.<sup>29</sup>

Dehydrins lack cysteine and tryptophan residues and are characterized by the presence of three conserved sequences: the K-segment, the S-segment, and the Y-segment. Dehydrins fall into one of five classes ( $K_n$ ,  $SK_n$ ,  $K_nS$ ,  $Y_nSK_2$ , and  $Y_2K_n$ ) based on the combination of K-, S-, and Y-segments that they contain (reviewed in refs 3, 6, and 8). The S-segments, as well as the adjacent serine and tyrosine residues flanking these segments, are predicted to be putative sites of phosphorylation for kinases such as CKI (casein kinase I), CKII (casein kinase II), and PKC (protein kinase C).<sup>15,20,22,23,30,31</sup> Reversible phosphorylation is

**Received:** August 3, 2011

**Revised:** October 1, 2011

**Published:** October 4, 2011

an important post-translational modification in eukaryotic organisms, which provides a regulatory mechanism for controlling the activity, function, and/or translocation of proteins.<sup>18,32,33</sup> Dehydrin ERD14, which accumulates in *Arabidopsis* during early responses to dehydration, is phosphorylated in vivo, and four CKII phosphorylation sites for this protein have been identified in vitro.<sup>23</sup> Dehydrin RAB17 has also been shown to be phosphorylated in vivo.<sup>34,35</sup>

In several cases, it has been shown that dehydrin phosphorylation promotes ion binding.<sup>22,23</sup> For instance, dephosphorylation of the vacuole membrane-associated protein VCaB45 by alkaline phosphatase weakened its ability to bind Ca<sup>2+</sup>; when phosphorylated by CKII in vitro, the protein regained its ability to bind Ca<sup>2+</sup>.<sup>22</sup> Similarly, the ion binding property of ERD10 was demonstrated to be enhanced by phosphorylation.<sup>23</sup> It has been shown that the phosphorylation-regulated ion binding activity is generally conserved in the acidic subfamily of dehydrins. For instance, acidic *Arabidopsis* COR47 and ERD10 possess ion binding properties similar to those of ERD14,<sup>11</sup> and their ability to bind metal ions is prevented by treatment with shrimp alkaline phosphatase.

On the basis of amino acid alignments, COR47, ERD10, and ERD14 are 43% similar in sequence in their S-segments and in the immediate regions surrounding the S-segments. Mutation in this region prevented phosphorylation as well as binding to Ca<sup>2+</sup>. A dehydrin lacking an S-segment, XERO2, could not be phosphorylated and did not bind to Ca<sup>2+</sup>, providing evidence that the S-segment may be essential for the ion binding properties of dehydrins.<sup>11</sup> Because the amphipathic  $\alpha$ -helices of the K-segments of dehydrins are adjacent to the sites of phosphorylation, this post-translational modification may regulate the intra- and intermolecular interactions between hydrophobic sites, which, in turn, may play a role in the polymerization and/or stabilization of cytoskeletal proteins. In particular, dehydrin ERD10 has been shown to associate with actin stress fibres in transfected rat fibroblasts,<sup>16</sup> and it is suggested below that plant dehydrins, in general, may associate with actin in specific physiological roles.

Dehydrins TsDHN-1 and TsDHN-2 are homologues of dehydrin RAB18, which was first investigated by Wong and colleagues.<sup>36</sup> Both of these proteins are of the Y<sub>n</sub>SK<sub>2</sub> class, although the former is acidic (calculated pI of 5.25 and M<sub>r</sub> of 30140.3 Da) and the latter slightly basic (calculated pI of 7.91 and M<sub>r</sub> of 21435.1 Da). We have previously reported that TsDHN-1 and TsDHN-2, originally isolated from *Thellungiella salsuginea* (salt cress, also called *Thellungiella halophila*), a close relative of *Brassica* spp., gain secondary structure upon association with large unilamellar vesicles (LUVs) that mimic the plant plasma membrane in vitro.<sup>8,9</sup> This plant is a crucifer that thrives in the Canadian sub-Arctic (Yukon Territory) where it grows on saline-rich soils and experiences periods of both extreme cold and drought and has been proposed as a valuable new model plant for research on abiotic stress tolerance.<sup>37,38</sup> We have thus begun to study the structural characteristics of TsDHN-1 and TsDHN-2 to improve our understanding of their functions in facilitating cold and drought tolerance in *T. salsuginea*,<sup>8,9</sup> roles that may be anticipated to extend significantly beyond membrane stabilization.

In this investigation, we have examined how phosphorylation of TsDHN-1 and TsDHN-2 can affect their structures, alter their ability to polymerize and stabilize actin, and also alter their ability to bind divalent cations Ca<sup>2+</sup> and Zn<sup>2+</sup>. Using circular dichroism (CD) spectroscopy, we show that both phosphory-

lated TsDHN-1 and TsDHN-2 gain polyproline II (PPII) structure with a decrease in temperature, a conformation adopted by many intrinsically disordered proteins for interactions with various ligands.<sup>39</sup> Using attenuated total reflection-Fourier transform infrared (ATR-FTIR) spectroscopy, we demonstrate that phosphorylation induces ordered secondary structure in each membrane-associated protein (induced folding) and that association of Zn<sup>2+</sup> does not further induce significantly more ordered secondary structure in phosphorylated TsDHN-1 and TsDHN-2, as seen in unphosphorylated TsDHN-1 and TsDHN-2. We also investigate the stabilization of actin filaments by phosphorylated TsDHN-1 and TsDHN-2 by a fluorescence-based polymerization assay, transmission electron microscopy, and atomic force microscopy. We observe that only phosphorylated TsDHN-1 and TsDHN-2 polymerize actin filaments. These results suggest that phosphorylation of TsDHN-1 and TsDHN-2 may enhance or alter their interactions with the cytoskeleton, which, in turn, may stabilize organellar and plasma membranes in vivo, thus mitigating the effects of environmental stresses experienced by this organism.

## MATERIALS AND METHODS

**Materials.** Chemicals used for these studies were reagent grade unless otherwise stated and were acquired from either Fisher Scientific (Unionville, ON) or Sigma-Aldrich (Oakville, ON). Electrophoresis grade chemicals were purchased from ICN Biomedicals (Costa Mesa, CA) or Bio-Rad Laboratories (Mississauga, ON). The Ni<sup>2+</sup>-NTA (nitrilotriacetic acid) agarose beads were purchased from Qiagen (Mississauga, ON). Heavy water (D<sub>2</sub>O) was obtained from Cambridge Isotope Laboratories (Andover, MA). The lipids phosphatidylcholine (PC), phosphatidylethanolamine (PE), phosphatidylglycerol (PG), dimyristoylphosphatidylglycerol (DMPG), phosphatidylinositol (PI), phosphatidylserine (PS), and cholesterol (Chol) were obtained from Avanti Polar Lipids (Alabaster, AL). The lipids digalactosyldiacylglycerol (DGDG), monogalactosyldiacylglycerol (MGDG), and sulfoquinovosyl diacylglycerol (SQDG) were obtained from Lipid Products (Nutfield Nurseries, Redhill, Surrey, U.K.).

**Overexpression and Purification of Recombinant Dehydrin.** The previously described pTYB2TsDHN-1 and pTYB2TsDHN-2 vectors<sup>8,9</sup> were used as template DNA to perform polymerase chain amplification reactions (PCR) to generate inserts for TsDHN-1 and TsDHN-2 (GenBank accession numbers 1347304 and DN776754.1, respectively). The PCRs that yielded cDNA product encoding the full-length coding region of TsDHN-1 and TsDHN-2 were TA-cloned into the Champion pET-SUMO Expression System (Invitrogen Life Technologies, Burlington, ON). All synthetic oligonucleotides were purchased from the Laboratory Services Division (University of Guelph). For insert amplification of TsDHN-1, the following oligonucleotide primers were used: 5'-ATGGCG-GAAGAGTACAAGAACG-3' and 5'-TAAGCATCA-GACTCTTTTC-3'. For the TsDHN-2 insert, the following oligonucleotide primers were used: 5'-ATGGCGTCTTACCA-GAACCG-3' and 5'-TTAACGACCACCACCCAGG-3'. All PCRs were performed using Taq polymerase (Invitrogen Life Technologies) using the following cycle parameters: initial denaturation temperature of 92 °C for 10 min, 25 cycles of 92 °C for 1 min, 55 °C for 30 s, and 72 °C for 2 min, followed by a final extension of 72 °C for 7 min. The PCR products were cloned directly into the pET-SUMO vector, and 1  $\mu$ L from

each ligation reaction mixture was transformed into One Shot TOP10 Chemically Competent *Escherichia coli* (Invitrogen Life Technologies). Several bacterial colonies were inoculated; the plasmids were isolated using the High Pure Plasmid Isolation Kit (Roche Applied Sciences), and positive plasmids were confirmed by sequencing (Laboratory Services Division, University of Guelph). Subsequent plasmids encoding the SUMO–TsDHN fusion proteins were transformed into *E. coli* BL21-CodonPlus(DE3)pLysS cells (Stratagene, La Jolla, CA) for overexpression and purification.

A 20 mL Luria-Bertani overnight culture, containing 30  $\mu\text{g}/\text{mL}$  kanamycin (Kan) and 34  $\mu\text{g}/\text{mL}$  chloramphenicol (Cam), was inoculated using a single *E. coli* colony transformed with either the pET-SUMO-TsDHN-1 or pET-SUMO-TsDHN-2 plasmid. The following day, the 20 mL culture was transferred to 1.5 L of 2 $\times$ YT (yeast-tryptone) medium containing the same concentration of antibiotics and grown at 37 °C to an optical density (600 nm) of 0.4–0.6. From here, the cultures were induced for 3 h with 1 mM IPTG (isopropyl  $\beta$ -D-thiogalactopyranoside). The cell pellet was then collected by centrifugation (6371g for 10 min at 4 °C) and resuspended in 45 mL of lysis buffer [1 $\times$  PBS (2 mM KH<sub>2</sub>PO<sub>4</sub>, 8 mM Na<sub>2</sub>HPO<sub>4</sub>, 137 mM NaCl, and 2.7 mM KCl) containing 150 mM NaCl, 10 mM imidazole, and 1% (v/v) Triton X-100 (pH 8.0)]. The cells were homogenized, and 45  $\mu\text{L}$  of 1 M PMSF (phenylmethanesulfonyl fluoride) dissolved in dimethyl sulfoxide (DMSO) was added to the lysate. The lysate was stirred on ice for 40 min and frozen for 1 h at –20 °C. It was then thawed and centrifuged at 27216g for 30 min at 4 °C. The supernatant was collected and stored at –20 °C until it was used.

The Ni-NTA column was prepared with a bed volume of 4.5 mL [9 mL of a 50% slurry solution (Qiagen)]. All solutions added to the column were filtered with a 0.45  $\mu\text{m}$  filter (Millipore, Etobicoke, ON). The column was first equilibrated with 45 mL of lysis buffer before the crude lysate was loaded. The column was washed with 40 mL of wash buffer 1 [1 $\times$  PBS containing 150 mM NaCl and 10 mM imidazole (pH 8.0)] and then with 40 mL of wash buffer 2 [1 $\times$  PBS containing 15 mM imidazole (pH 8.0)]. The protein was eluted in 1.4 mL fractions with 28 mL of elution buffer [1 $\times$  PBS containing 500 mM imidazole (pH 8.0)]. The absorbance at 280 nm was measured for each fraction.

To determine the purity of the protein and confirm the elution fractions containing protein, the samples were analyzed via 12% sodium dodecyl sulfate–polyacrylamide gel electrophoresis (SDS-PAGE). The fractions containing protein were combined and diluted to 50 mL with dialysis buffer [1 $\times$  PBS with 10% glycerol (pH 8.0)]. The protein was then loaded into presoaked dialysis tubing [6000–8000 molecular weight cutoff (MWCO) (Fisher Scientific, Ottawa, ON)] and dialyzed for 12 h in 2 L of dialysis buffer, with one change of buffer. After dialysis, the absorbance at 280 nm was read to estimate the concentration of protein using an extinction coefficient of 0.058 M<sup>–1</sup> cm<sup>–1</sup> for SUMO-tagged TsDHN-1 and 0.404 M<sup>–1</sup> cm<sup>–1</sup> for SUMO-tagged TsDHN-2. The primary sequence analysis suite at <http://www.expasy.org/tools/aladente/> was used to calculate these extinction coefficients in 6.0 M guanidine hydrochloride and 0.02 M phosphate buffer (pH 6.5).

Recombinant SUMO protease was expressed from a pET28b plasmid (Novagen, Gibbstown, NJ) containing His-tagged Ulp(403–621), which was a kind gift from C. Lima (Sloan-Kettering Institute, New York, NY).<sup>40</sup> Protease digestion was

performed using 1  $\mu\text{g}$  of protease per 1000  $\mu\text{g}$  of protein. Additionally, 2 mM dithiothreitol (DTT) was added to the digestion mixture. The mixture was incubated at 30 °C for 3 h. Samples were taken at the beginning and then at several time points during the digestion. Analysis by SDS-PAGE (12% separating and 5% stacking gel) was used to confirm a complete digestion.

After cleavage of the SUMO fusion protein, the mixture was passed through another Ni-NTA column to separate the protease and SUMO tag from the protein of interest. The 4.5 mL Ni-NTA column was equilibrated with 40 mL of equilibration buffer [1 $\times$  PBS containing 150 mM NaCl and 10 mM imidazole (pH 8.0)]. The digestion mixture was loaded onto the column and washed with 30 mL of wash buffer 1. The column was washed again with wash buffer 2. Finally, 30 mL of elution buffer was added to the column to elute all bound proteins. Samples from all steps were analyzed by SDS-PAGE (12% separating and 5% stacking gel) to determine the presence and purity of the protein of interest.

The fractions containing protein were combined and loaded into presoaked dialysis tubing [6000–8000 MWCO (Fisher Scientific, Ottawa, ON)]. Four changes of 50 mM ammonium bicarbonate and two changes of heavy water were used for dialysis. The samples were then filtered using a 0.45  $\mu\text{m}$  filter to remove precipitated protein and then frozen at –80 °C before lyophilization.

#### In Vitro Phosphorylation of TsDHN-1 and TsDHN-2.

For in vitro phosphorylation, 60 nmol (1.8 mg) of TsDHN-1 or 90 nmol (1.8 mg) of TsDHN-2 in kinase buffer [20 mM Tris-HCl, 0.35 M NaCl, 1 mM EDTA, 10 mM MgCl<sub>2</sub>, and 2 mM DTT (pH 7.5)] reacted with 600 nmol of ATP in the presence of 20 or 30 units of CKII (BIOMOL Research Laboratories, Plymouth Meeting, PA), respectively. The reaction proceeded first at 30 °C for 5 h and was continued overnight at 4 °C. For phosphoprotein analysis, polyacrylamide gels containing protein mixtures were fixed overnight with 100 mL of 50% methanol with 10% acetic acid. After removing excess methanol and acetic acid by rinsing the gels twice with Milli-Q water, we stained the fixed gels with ProQ Diamond (Molecular Probes, Invitrogen Life Technologies) gel stain for 90 min and then destained the gels with 20% acetonitrile and 50 mM sodium acetate (pH 4.0). The ProQ Diamond stain specifically binds to proteins with phosphate groups on serine, threonine, and tyrosine residues, allowing their detection by fluorescence.<sup>41</sup> Stained gels were visualized with a Typhoon 9400 variable imager (Amersham Biosciences, Sunnyvale, CA) at 620 nm with excitation at 532 nm. The gels were stained subsequently with Sypro Ruby stain (Molecular Probes, Invitrogen Life Technologies) for total protein detection.<sup>42</sup> The phosphorylation of each dehydrin was further confirmed and quantified by mass spectrometry (Protein Analysis Facility, Hospital for Sick Children, Toronto, ON).

**Reversed-Phase HPLC.** Reversed-phase high-performance liquid chromatography (HPLC) was employed to assess the final purity of the TsDHN-1 and TsDHN-2 proteins and for the recovery of phosphorylated TsDHN-1 and TsDHN-2, following the purification procedure. Our previously published protocol was used, with minor modifications.<sup>43,44</sup> The HPLC system comprised a Waters 626 gradient pump, a Waters 2487 variable-wavelength dual-channel UV detector, a 2 mL sample loop (50  $\mu\text{L}$  sample loop used for assessing purity), and a Waters Symmetry 300 C18 column (5  $\mu\text{m}$ , 4.6 mm diameter  $\times$  150 mm length). The column was maintained at 25 °C, and the

absorbance at 214 nm was followed for detecting a pure protein fraction. The flow rate was maintained at 1 mL/min. Acetonitrile and trifluoroacetic acid (TFA) were used as the mobile phase and ion pairing agent, respectively. After a loading time of 2 min at 10% acetonitrile and 0.1% TFA, the linear elution gradients started from 10 to 50% acetonitrile, and 0.1% trifluoroacetic acid, at a rate of 1% acetonitrile per minute, followed by 5% acetonitrile per minute for an additional 10 min.

**Circular Dichroism Spectroscopy.** The effects of pH, phosphorylation, temperature, and divalent cations on protein secondary structure in buffer alone [20 mM Tris-HCl (pH 7.3) and 100 mM NaCl] were studied by CD spectroscopy on a JASCO J-815 spectropolarimeter (Japan Scientific, Tokyo, Japan), equipped with a recirculating water bath. Both proteins were used at a concentration of 1.5 mg/mL [0.049 mM for TsDHN-1 ( $M_r = 30.1$  kDa) and 0.070 mM for TsDHN-2 ( $M_r = 21.4$  kDa)]. The scan rate was 50 nm/min, and the band resolution was 1 nm. The sample volume was 70  $\mu$ L in a demountable quartz cuvette with a path length of 0.01 cm. The CD experiments in the presence of Zn<sup>2+</sup> or Ca<sup>2+</sup> were conducted with a molar protein:Zn<sup>2+</sup> or protein:Ca<sup>2+</sup> ratio of 1:10, to ensure saturation of all binding sites. The CD spectra were recorded from 5 to 45 °C with 10 °C intervals. Six successive scans were recorded; the sample blank was subtracted, and the scans were averaged. The data averaging and smoothing (using the Savitzky–Golay algorithm) operations were accomplished with OriginPro (version 8, OriginLab Corp., Northampton, MA). All CD spectroscopic experiments were performed in triplicate, and representative spectra are presented.

**Lipid Vesicle Preparation and Protein Reconstitution for ATR-FTIR Spectroscopy.** Lipid stocks were prepared in chloroform at the desired mass ratio. The solvent was then evaporated under a mild flow of nitrogen gas. The residual solvent was removed by keeping the sample under vacuum overnight. Lipid mixtures (10 mg) were rehydrated in 1 mL of buffer [20 mM Tris-HCl (pH 7.3) and 100 mM NaCl] at room temperature overnight with vigorous shaking. To prevent lipid oxidation, lipid mixtures were flushed with nitrogen gas. To increase the efficiency of entrapment of water-soluble compounds, hydrated lipid suspensions were subjected to three freeze–thaw cycles by alternately placing the vials in a –20 °C freezer for 40 min and then in a 45 °C water bath for 30 min with occasional vortexing.

Large unilamellar vesicles (LUVs) were formed by extruding lipid mixtures (61 times at 45 °C) through a polycarbonate membrane with a 100 nm pore size. The lipid compositions were chosen so that they mimicked plasma (33:47:20 PC:PS:PI weight ratio), or chloroplast (51:26:7:3:9:1 MGDG:DGDG:SQDG:PC:DMPG:PI weight ratio) plant membranes, as we have previously described.<sup>8,9</sup> The sizes of vesicles were measured to be approximately 100 nm, using a dynamic light scattering (DLS) Zetasizer Nano-S model ZEN1600 instrument (633 nm “red” laser; Malvern Instruments, Southboro, MA).

For reconstitution, the desired amount of protein [in 20 mM Tris-HCl (pH 7.3) 100 mM NaCl] was added to the LUVs at a lipid:protein weight ratio of 1:1. The protein–LUV complexes were used within 1 h of preparation for ATR-FTIR measurements. The lipid:protein ratio was chosen to ensure a significant signal-to-noise ratio.

First, 5 mM Zn<sup>2+</sup> in 20 mM Tris-HCl (pH 7.3) and 100 mM NaCl was added to the protein solution to achieve a concentration of 0.36 mM for phosphorylated TsDHN-1 and 0.48 mM for phosphorylated TsDHN-2 (to reach the molar zinc:protein ratio of 10:1). After incubation of the proteins with Zn<sup>2+</sup> for 5 min at room temperature, LUVs were added to reach a protein:lipid weight ratio of 1:1, followed by a further incubation for 10–15 min at room temperature. Following this incubation, the protein–LUV complexes (with or without Zn<sup>2+</sup>) were centrifuged in a table-top centrifuge (18000g) for 1 h. After the supernatant had been removed, the aggregate was used for ATR-FTIR analysis.

**Attenuated Total Reflection-Fourier Transform Infrared (ATR-FTIR) Spectroscopy.** The effects of Zn<sup>2+</sup> on the protein secondary structure when the Zn<sup>2+</sup> is associated with membranes were studied with a Bruker Optics IFS 66v/S FTIR spectrometer equipped with a liquid nitrogen-cooled mercury cadmium telluride (MCT) detector. A vertical PIKE MIRacle Micro ATR accessory (PIKE Technologies, Madison, WI) combined with a one-reflection diamond ATR crystal unit with a diameter of 6 mm was used. The crystal was cleaned with 2-propanol, followed by MilliQ H<sub>2</sub>O. The crystal surface was dried under nitrogen before being used. All experiments were conducted at room temperature (~22 °C). For each spectrum, 1000 interferograms were collected and Fourier-transformed to give a resolution of 2  $\text{cm}^{-1}$ . To minimize the spectral contributions from atmospheric water vapor, the optic and sample compartments of the spectrometer were evacuated continuously with dry nitrogen.

Aliquots of ~30  $\mu$ L of this protein–lipid complex solution were added onto a one-reflection diamond ATR crystal one at a time, followed by a 45 min incubation in a desiccator under vacuum to yield a dry film. A second layer of deposition was necessary to yield a high signal:noise ratio spectrum with the amide I signal around 0.6 OD (optical density) unit. Spectra ranging from 950 to 1750  $\text{cm}^{-1}$  were recorded while a stream of nitrogen gas, containing rich D<sub>2</sub>O vapor, flowed over the sample on the crystal with the aid of a home-built bubbler. The spectra, recorded after the complete H<sub>2</sub>O–D<sub>2</sub>O exchange, were used for secondary structure analysis. The completion of H<sub>2</sub>O–D<sub>2</sub>O exchange was confirmed when the spectra in the amide II region did not change further. A typical measurement needed approximately 90–120  $\mu$ g of either phosphorylated TsDHN-1 or TsDHN-2. All ATR-FTIR spectroscopic experiments were performed in triplicate, and representative spectra are presented.

**ATR-FTIR Data Analysis.** The overlapping bands in the ATR-FTIR spectra were resolved by Fourier self-deconvolution (FSD) using OMNIC (Thermo Fisher Scientific, Waltham, MA). The bandwidth at half-height was set to 15  $\text{cm}^{-1}$ , and the enhancement value was set to 1.8. The number and location of peaks of the secondary structure components were verified by the second-derivative method using PeakFit (version 4.12, Seasolve Software, San Jose, CA). The conditions were chosen to minimize the increase in noise, and the appearance of side chain lobes, while achieving maximum band narrowing.

The wavenumbers of these component bands were subsequently used in PeakFit as input parameters for curve fitting analysis of the amide I original spectrum. The parameters were left free to adjust iteratively, with each wavenumber restricted to vary within a range of  $\pm 2 \text{ cm}^{-1}$ .<sup>8,9</sup> The amide I region (~1600 to ~1700  $\text{cm}^{-1}$ ) arises because of the peptide backbone and some side chain C=O stretching, and some in-

plane N–H bending in a pure H<sub>2</sub>O environment. Because all the FTIR measurements were conducted here in a saturated D<sub>2</sub>O environment, the band located between 1600 and 1700 cm<sup>-1</sup> can be considered to be due to C=O stretching only.

**Purification of Actin from Chicken Muscle.** Actin was extracted from chicken muscle acetone powder using an established protocol.<sup>45</sup> Briefly, acetone is used to extract protein from chicken muscle, yielding a powder that is washed with chloroform to remove lipids. Actin can be induced to undergo reversible polymerization in vitro. G-Actin (globular actin) is stable in G-buffer [2 mM Tris-HCl (pH 8.0), 0.2 mM ATP, 0.2 mM CaCl<sub>2</sub>, and 0.2 mM 2-mercaptoethanol], whereas F-actin (fibrous actin or microfilaments) can be formed in F-buffer (G-buffer with the addition of 50 mM KCl, 1 mM EGTA, and 2 mM MgCl<sub>2</sub>). By successive cycles of actin polymerization followed by high-speed centrifugation, actin can be extracted to a high degree of purity from muscle acetone powder.<sup>45</sup> Here, the purity of G-actin obtained after two successive cycles of polymerization and depolymerization was checked using MALDI-TOF mass spectrometry, supported by SDS-PAGE, and no further purification steps were required, consistent with our previous experience using this procedure.<sup>44,46</sup>

To prevent proteolytic activity of G-actin during extraction, all solutions used in the extraction procedure were freshly prepared. The concentration of G-actin was estimated by measuring the absorbance of the solution at 280 nm and applying an extinction coefficient of 0.62 L g<sup>-1</sup> cm<sup>-1</sup> as previously used.<sup>47</sup> Actin suspended in depolymerization buffer or G-buffer was aliquoted into 1 mL microfuge tubes, flash-frozen in liquid nitrogen, and stored at -80 °C. The labeling of actin with pyrene was performed as we have previously described.<sup>46</sup>

**Actin Polymerization Assay.** To study dehydrin-induced actin polymerization in vitro, we added 15 μM actin in G-buffer with 5% of it labeled with pyrene to 60 μM TsDHN-1 or TsDHN-2 or phosphorylated TsDHN-1 or TsDHN-2 in G-buffer to yield a final actin concentration of 5 μM and final dehydrin concentrations ranging from 0 to 24 μM. The molar ratios of actin to dehydrin thus ranged from 1:0 to 1:4.8. As a control, actin polymerization (formation of microfilaments or F-actin) could also be induced in vitro by F-buffer (G-buffer with additional 50 mM KCl, 1 mM EGTA, and 2 mM MgCl<sub>2</sub>) alone. The polymerization of actin was followed by measuring the change in the fluorescence intensity of pyrene-labeled actin employing an automated microplate fluorescence reader (Polarstar Omega; BMG Labtech GmbH, Offenburg, Germany), using a 367–10 nm filter for the excitation channel and a 405–10 nm filter for the emission channel. After the plate had been shaken for 30 s, the emission intensity was measured for 40 min at 27 °C.

The effect of unphosphorylated TsDHN on phosphorylated TsDHN-induced actin polymerization was determined using a previously described spectroscopic method.<sup>48</sup> Briefly, to 3.3 nmol of G-actin in 1800 μL of G-buffer was added 9.9 or 13.2 nmol of phosphorylated TsDHN-1 or TsDHN-2 in 100 μL of G-buffer, for the evaluation of different dehydrin:actin molar ratios, and we followed the increase in pyrene fluorescence intensity (excitation at 365 nm and emission at 410 nm), using a Photon Technology International (London, ON) Alphascan-2 spectrophotometer, until a plateau was achieved. Then 9.9 nmol of unphosphorylated TsDHN-1 or TsDHN-2 in 100 μL of G-buffer was added, and the emission was measured for an additional 30 min. The samples were stirred continuously

during the measurements. The experiment was performed at 27 °C, and the final actin:Phos-TsDHN:TsDHN molar ratio was 1:3:3 or 1:4:3.

**Transmission Electron Microscopy.** Transmission electron microscopy was applied to study the morphology of the actin assembly affected by unphosphorylated and phosphorylated TsDHNs. Samples were prepared as previously described.<sup>44,46</sup> Briefly, 5 μM G-actin was allowed to interact with unphosphorylated or phosphorylated TsDHN in G-buffer, at an actin:dehydrin molar ratio of 1:3 or 1:4, for 40 min at 27 °C. In some cases, F-buffer or unphosphorylated TsDHN was added to the polymerized G-actin. Samples were adsorbed onto 200-mesh Formvar-coated copper grids, stained with 2% uranyl acetate, and blotted dry before being examined immediately with a Philips (Eindhoven, The Netherlands) CM10 transmission electron microscope.

**Actin Bundling and Actin–TsDHN Binding.** The binding to and bundling of actin by dehydrin were studied using a sedimentation assay that we have previously used to study cytoskeletal assembly by myelin basic protein.<sup>44,46</sup> Here, different variants of dehydrin (unmodified TsDHN-1 or TsDHN-2 or phosphorylated TsDHN-1 or TsDHN-2) in G-buffer were added to actin in G-buffer to give a final actin:TsDHN molar ratio of 1:3.6 and a final volume of 100 μL. After incubation of the reaction mixtures for 1 h at 27 °C, the samples were centrifuged at either low speed (18000g) or high speed (100000g). Because only the dehydrins that were bound to assembled actin precipitated, and the unbound dehydrin or unbundled actin remained in the supernatant, the bound and unbound dehydrins could be differentiated. The low-speed centrifugation sedimented the highly bundled actin, whereas the high-speed centrifugation sedimented the polymerized F-actin, as well.

After 80 μL of supernatant of each sample had been transferred into separate microfuge tubes, the samples were mixed with 20 μL of 5× sample buffer [60 mM Tris-HCl (pH 6.8), 25% glycerol, 2% SDS, 14.4 mM β-mercaptoethanol, and 0.1% bromophenol blue]. The pellets were resuspended in 25 μL of 5× sample buffer, and a final volume of 100 μL was reached with 75 μL of Milli-Q H<sub>2</sub>O. Samples (20 μL) from both pellets and supernatants were boiled for 5 min and analyzed for the presence of dehydrin and actin by 14% discontinuous SDS-PAGE.<sup>44,46</sup> Following electrophoresis, the gels were stained for 20 min [10% (v/v) acetic acid, 45% (v/v) methanol, and 0.1% (w/v) Coomassie Blue R-250] and destained [10% (v/v) acetic acid and 10% (v/v) methanol] overnight.

**Atomic Force Microscopy.** Samples were prepared as described above followed by fixation with 1% glutaraldehyde for 30 s. Fifty microliters of a sample was adsorbed onto a freshly cleaved mica or silicon wafer spin coated with poly(methyl methacrylate) (PMMA). Unattached actin assembles were rinsed with Milli-Q H<sub>2</sub>O. The samples were imaged in 20 mM Tris-HCl buffer (pH 7.3) in tapping mode with an Agilent 5500 SPM (Agilent Technologies, Palo Alto, CA) closed-loop small scanner with a lateral scan range of 10 μm × 10 μm. A tapping mode tip with a spring constant of 42 N m<sup>-1</sup> (Nanoworld Innovative Technologies, Neuchâtel, Switzerland) and a homemade fluid cell were used for imaging in liquid. Imaging was performed with typical resonance frequencies of 53–54 kHz in buffer and scanning rates of 2–3 kHz to avoid detrimental effects on the morphology of samples. Topography, amplitude, and phase mode images were obtained simulta-

neously at an ambient temperature to allow a good understanding of the samples. However, quantitative information was obtained from the topographic images only.

## RESULTS

**Overexpression and Purification of TsDHNs.** One of the many methods for preventing *in vivo* degradation and obtaining good yields of recombinant proteins or short polypeptides during expression in prokaryotic cells (*E. coli*) is to express them as fusion proteins from which target proteins or peptides can be released by enzymatic cleavage. Here, we used the small ubiquitin-related modifier (SUMO) linked with a hexahistidine tag to overexpress the *T. salsuginea* dehydrins TsDHN-1 and TsDHN-2 in *E. coli* BL21-CodonPlus(DE3)RP cells. The SUMO fusion expression system is generally used to increase the solubility of overexpressed proteins in bacterial systems. A hexahistidine tag on the N-terminus of SUMO facilitates purification, and the SUMO tag at the N-terminus of the protein of interest can subsequently be cleaved. The advantages of this expression system lie in its simplicity and ability to produce isotopically labeled peptides at relatively high yield, without any additions related to the purification protocol.<sup>49,50</sup> We have previously used this expression system to produce recombinant peptide fragments of myelin basic protein with high yields for structural and functional studies.<sup>44</sup>

Here, the cDNAs encoding TsDHN-1 and TsDHN-2 were cloned into the Champion pET-SUMO Expression System. Plasmids that were confirmed by sequencing to encode the TsDHN-1 and TsDHN-2 proteins were transformed into *E. coli* BL21-CodonPlus(DE3)pLysS cells (Stratagene) and expressed in 2×YT (pH 7.3) (Figure S1 of the Supporting Information). Pure recombinant proteins containing the His<sub>6</sub>-SUMO tag at their N-termini were obtained from the lysates of the harvested cells by application of affinity-based chromatography with a Ni<sup>2+</sup>-NTA column (Figure 1A,B). The SUMO tag was successfully cleaved by digestion with SUMO protease for 3 h and was separated from the pure proteins by application of a second affinity-based chromatography with a Ni<sup>2+</sup>-NTA column. During this second subtractive chromatography step, the cleaved SUMO tag along with the SUMO protease bound to the column, because they both contained hexahistidine affinity tags, whereas the untagged dehydrins of interest were recovered in the flow-through (F.T.) and wash fractions. The efficiency of proteolytic cleavage was evaluated by SDS-PAGE; it should be noted that aberrant migration of these dehydrins on these gels is characteristic of IDPs (Figure 1).<sup>19</sup> The yield of dehydrins was ~15 mg from 1 L of culture, which is much higher than the yield obtained by us previously with the purification method using IMPACT (intein-mediated purification with an affinity chitin-binding tag) affinity chromatography.<sup>8,9</sup>

**Phosphorylation of TsDHNs.** Phosphorylation sites in TsDHN-1 and TsDHN-2 are predicted to reside on large numbers of serine and threonine residues, based on several eukaryotic protein phosphorylation site prediction programs such as Netphos, NetphosK, and Scansite (<http://www.cbs.dtu.dk/services/NetPhosK/>). Dehydrins TsDHN-1 and TsDHN-2 were predicted by Netphos to contain 17 and 9 possible phosphorylation sites, respectively (results not shown). Both NetphosK and Scansite predicted that the most probable sites for phosphorylation by CKII were the seryl residue at position 124 in TsDHN-1 and the seryl residue at position 101 in TsDHN-2. We chose to use this kinase for *in vitro*

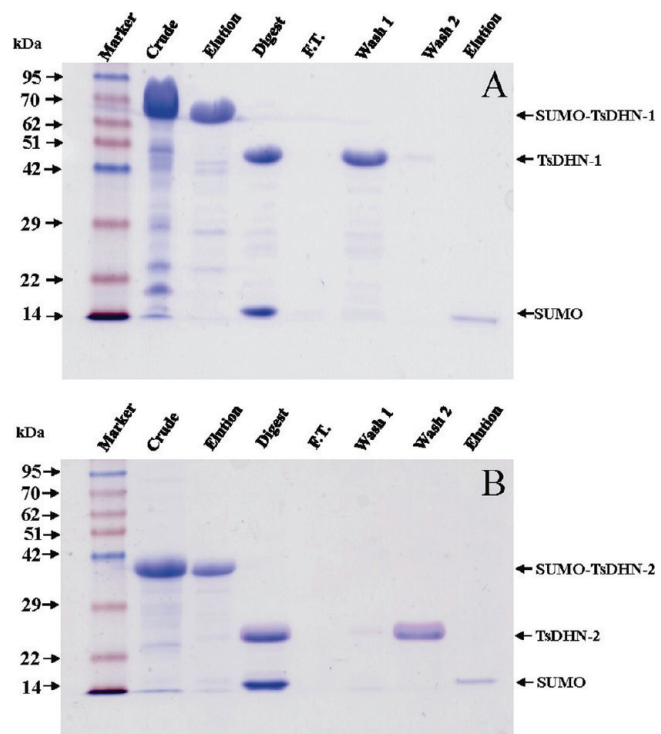


**Figure 1.** Purification of recombinant *T. salsuginea* dehydrins TsDHN-1 and TsDHN-2. Sodium dodecyl sulfate–polyacrylamide gel electrophoresis pattern of purification of (A) TsDHN-1 (major band at roughly 45 kDa, predicted  $M_r$  of 30140.3 Da) and (B) TsDHN-2 (major band at roughly 25 kDa, predicted  $M_r$  of 21435.1 Da) by Ni<sup>2+</sup>-NTA affinity chromatography. The abnormal migration of these dehydrins is characteristic of intrinsically disordered proteins<sup>19</sup> and is especially marked for TsDHN-1 because of its high net charge.<sup>8</sup> The molecular masses of markers are given in kilodaltons.

phosphorylation to be consistent with previous studies of other dehydrins.<sup>22,23</sup>

Here, the extent of phosphorylation of TsDHN-1 and TsDHN-2 *in vitro* by CKII was confirmed by phosphoprotein staining of a polyacrylamide gel containing the *T. salsuginea* proteins (results not shown) and by electrospray ionization (ESI) mass spectrometry (Figure S2 of the Supporting Information). The latter data indicate that there were predominantly two phosphorylation events for TsDHN-1 and predominantly one phosphorylation event for TsDHN-2. Dehydrin preparations such as these were used throughout the rest of this work to study the effects of phosphorylation on their secondary structure in diverse environments (aqueous environments at different pH values and temperatures and in membrane-associated form) and on their interactions with divalent cations and with actin.

**Effects of pH on Secondary Structures of TsDHNs.** In our previous studies, we have shown by CD spectroscopy that TsDHN-1 and TsDHN-2 in aqueous solution are mostly in a random coil conformation; ATR-FTIR spectroscopy revealed that they gained ordered secondary structure upon membrane and/or cation association.<sup>8,9</sup> Here, we have studied the effects of pH on the secondary structure compositions of TsDHN-1 and TsDHN-2 in buffer alone (Figure 2). We confirmed that both TsDHN-1 and TsDHN-2 are in a primarily random coil configuration at pH 7.3, which is indicated by the peak minima at ~200 nm. The peak minima shifted toward 205 nm at pH 6.4 and 5.8, suggesting that the protein becomes slightly more

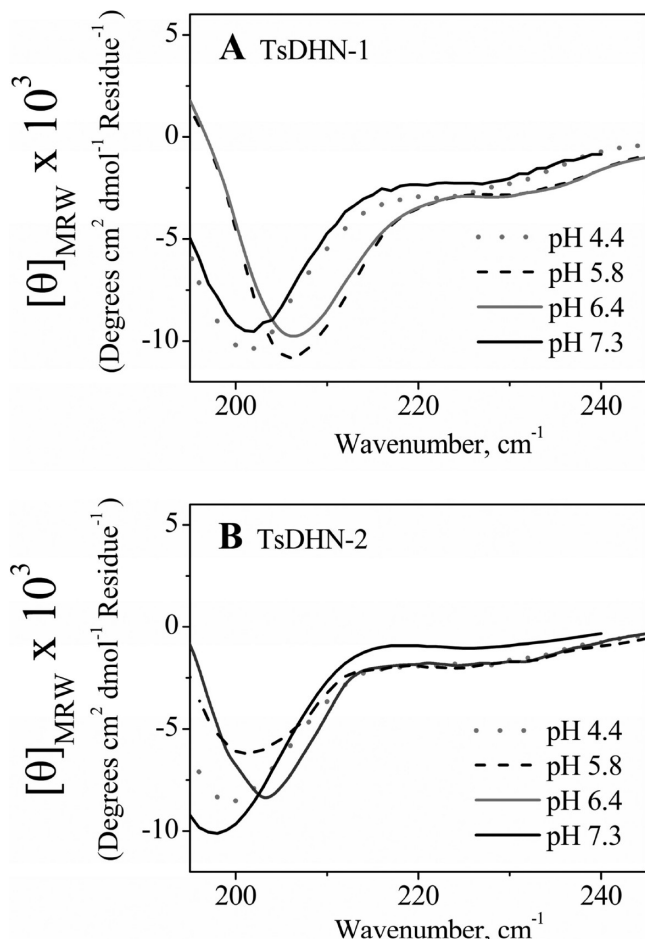


**Figure 2.** Effects of pH on the secondary structure composition of unmodified TsDHN-1 and TsDHN-2, studied by solution CD spectroscopy. Results are representative of experiments performed in triplicate.

ordered at these lower pH values. However, a further decrease in pH resulted in a shift of the peak minimum back to a shorter wavelength. Under normal conditions, the pH of the plant cytosol is ~7.5, whereas the pH of the apoplast and vacuolar lumen is 5.5. The pH of the cytosol declines during stress because of the shift in  $\text{Ca}^{2+}$  concentration.<sup>51,52</sup> The change in intracellular  $\text{Ca}^{2+}$  concentration is usually compensated by monovalent cations such as protons, and such changes in pH can act as a secondary messenger in response to stress in plants.<sup>53,54</sup> These considerations, and our results described here, suggest that dehydrins might undergo pH-induced conformational changes under stressful environmental conditions, thereby facilitating specific protein–protein interactions.

**Effects of Phosphorylation and Temperature on Secondary Structures of TsDHNS.** The CD spectra of unphosphorylated and phosphorylated TsDHN-1 and TsDHN-2 were first obtained at ambient temperature in Tris-HCl buffer and 100 mM NaCl (pH 7.3). The change in the secondary structure composition of TsDHN-1 and TsDHN-2 upon phosphorylation was not significant under these experimental conditions (Figure 3A,B).

Next, we evaluated the effects of temperature on the secondary structure composition of phosphorylated dehydrins, for comparison with our previous study of the unmodified

proteins in solution, in which we observed some cold stabilization of ordered structure.<sup>9</sup> An increase in the intensity of the positive band above 215 nm and a decrease in the intensity of the negative band around 200 nm were observed with a decrease in temperature for the phosphorylated TsDHNS, at both lower and higher pH values (Figure 3C–F). This observation indicates that low-temperature-induced folding is less pronounced in the phosphorylated TsDHNS than in the unphosphorylated TsDHNS that were studied in this way previously.<sup>9</sup> However, this feature is common in peptides containing polyproline type II (PPII) structures. In many cases, the negative minimum due to the  $\alpha$ -helical component masks the positive maximum at 223 nm. A temperature difference spectrum, obtained by subtracting the high-temperature spectrum from the low-temperature one, allows for the “amplification” of the signal from the PPII helix and is used to study both peptides and proteins (e.g., refs 55 and 56).

Here, the PPII conformation in TsDHN-1 and TsDHN-2 was sought by comparison of CD spectra over a range of temperatures. The PPII conformations are evident in both phosphorylated dehydrins as indicated by the minima near 197 nm and the maxima at approximately 215 nm in the difference spectra (insets in Figure 3C–F). The decrease in the differences in intensity at 220 and 197 nm with an increase in temperature is most probably due to an unfolding process, rather than to folding or to redistribution of the secondary structure components (Figure S3 of the Supporting Information). An isodichroic point is also observed at 208 nm, confirming a transition from random coil to PPII conformations. It has become apparent in recent years that the PPII conformation is an important component of intrinsically disordered proteins (reviewed in refs 39 and 56). The observations here of induced PPII conformations in these *T. salsuginea* dehydrins are suggestive of their multifunctionality and consistent with observations of this conformation in other dehydrin species.<sup>57</sup>

**Effects of Cations on Secondary Structures of Phosphorylated TsDHNS.** Cation binding has a significant effect on the secondary structure of phosphorylated TsDHNS. In the case of phosphorylated TsDHN-1, the addition of  $\text{Zn}^{2+}$  (Figure 4A,C) induced ordered secondary structure ( $\beta$ -turns) only at lower pH (pH 5.8). However, the addition of  $\text{Ca}^{2+}$  (Figure 4B,D) induced  $\beta$ -turns in phosphorylated TsDHN-1, regardless of pH. Only small changes in the secondary structure composition of phosphorylated TsDHN-2 were observed in the presence of  $\text{Zn}^{2+}$  (Figure 4E,G), although a gain in PPII conformation was observed in the presence of  $\text{Ca}^{2+}$  (Figure 4F,H). The secondary structures of phosphorylated TsDHNS were not significantly affected by temperature in the presence of  $\text{Zn}^{2+}$ .

In the presence of  $\text{Ca}^{2+}$ , the secondary structure of phosphorylated TsDHN-1 was also not significantly affected by temperature. However, the PPII conformation was enhanced at low temperatures in the case of phosphorylated TsDHN-2. Besides being an essential nutrient,  $\text{Ca}^{2+}$  also is an important secondary messenger during plant development as well as during various environmental stresses.<sup>58,59</sup> The change in pH and/or concentration of  $\text{Ca}^{2+}$  can also regulate the organization of the cytoskeleton.<sup>51</sup> Phosphorylation of dehydrins may thus serve to accentuate these responses *in vivo*.

**Secondary Structures of Phosphorylated TsDHNS in Association with Membranes.** The secondary structure compositions of unphosphorylated and phosphorylated

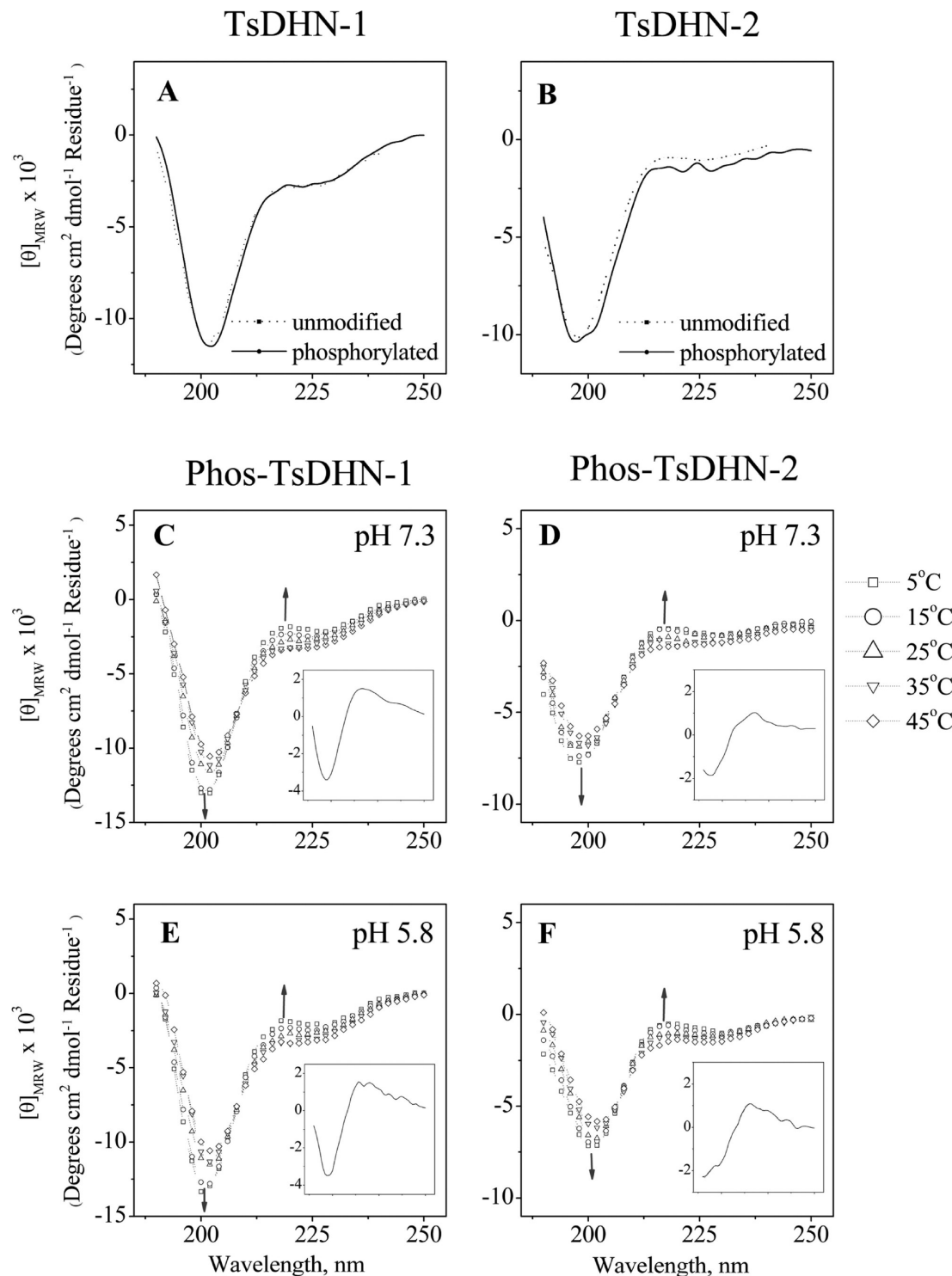


**Figure 3.** Effects of phosphorylation, temperature, and pH on the secondary structure composition of TsDHN-1 and TsDHN-2, studied by solution CD spectroscopy. (A and B) CD spectra showing the effect of phosphorylation on secondary structure. (C and D) CD spectra showing the effect of temperature on secondary structure at pH 7.3. (E and F) CD spectra showing the effect of temperature on secondary structure at pH 5.8. The difference spectra obtained by subtracting the CD spectra at 45 °C from the CD spectra at 5 °C are shown in the insets. Arrows show the direction of change with a decrease in temperature. Results are representative of experiments performed in triplicate.

TsDHN-1 and TsDHN-2 were investigated by ATR-FTIR spectroscopy when they were associated with LUVs with lipid compositions mimicking the plant plasma membrane (33:47:20 PC:PS:PI weight ratio) and chloroplast membrane (51:26:7:3:9:1 MGDG:DGDG:SQDG:PC:DMPG:PI weight ratio), as we have done previously.<sup>8,9</sup> The amide I band,

located between 1700 and 1600 cm<sup>-1</sup> in the FTIR spectra, is often used to estimate the secondary structure composition of proteins.<sup>60</sup> The different secondary structure components are usually hidden by the broadness of the bands in the raw FTIR spectra, and curve fitting and band narrowing methods are required to decompose them into different components.

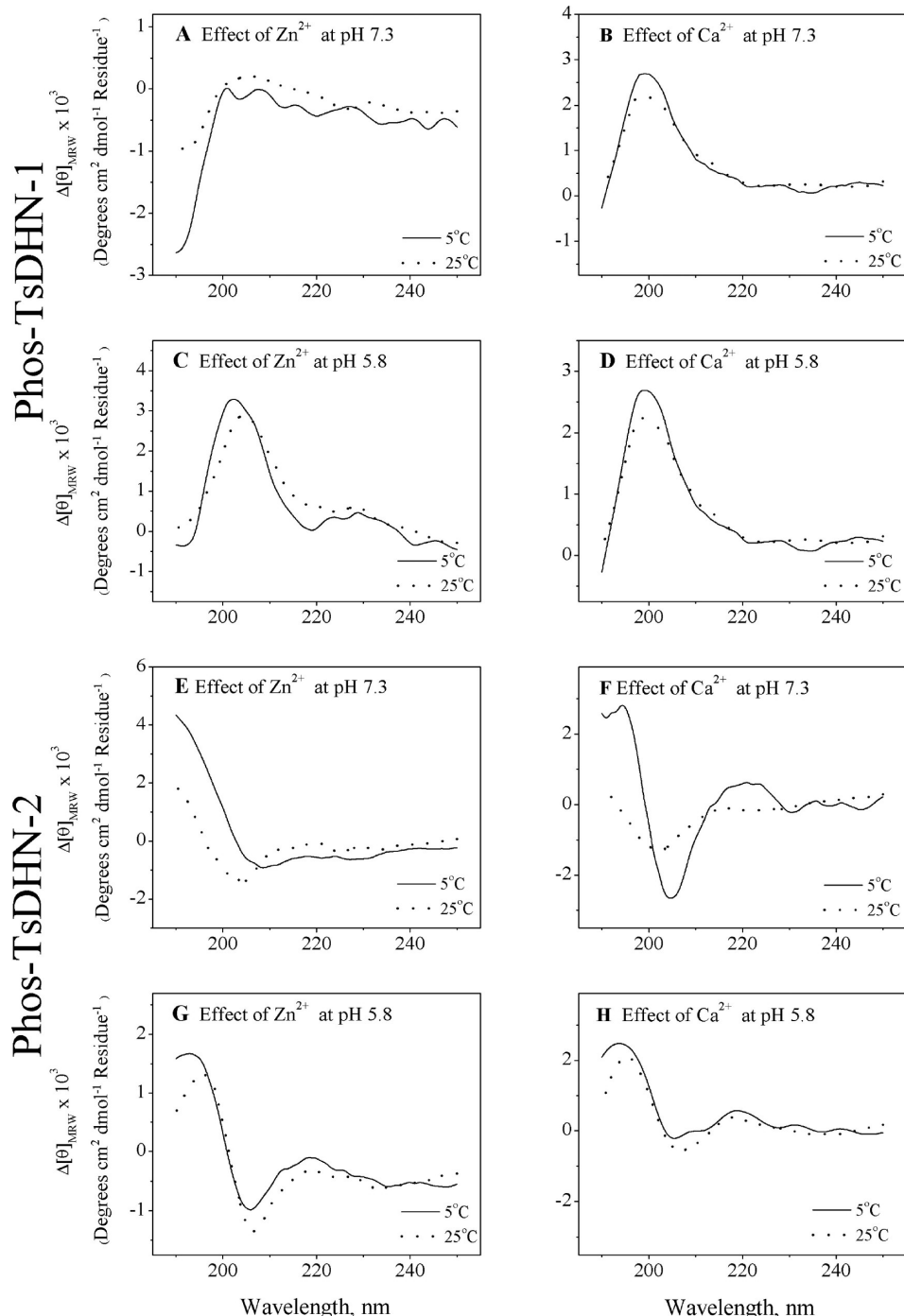


**Figure 4.** Effects of divalent cations on the secondary structure composition of phosphorylated TsDHN-1 and TsDHN-2, studied by solution CD spectroscopy. (A–D) Differences in CD spectra of phosphorylated TsDHN-1 in 20 mM HEPES-NaOH and 100 mM NaCl, obtained with or without cations at (A and B) pH 7.3 or (C and D) pH 5.8. (E–H) Differences in CD spectra of phosphorylated TsDHN-2 in 20 mM HEPES-NaOH and 100 mM NaCl, obtained with or without cations at (E and F) pH 7.3 or (G and H) pH 5.8. Results are representative of experiments performed in triplicate.

Nevertheless, there is considerable variability in published predictions,<sup>61</sup> as we have previously noted and reviewed.<sup>8,9</sup> For this reason, the changes in secondary structure compositions with different conditions, rather than overall compositions per se, are more important. Here also, the side chain contributions were not used to calculate secondary structures because the side chains of phosphorylated dehydrins appeared to be less exposed than in the unmodified proteins and thus potentially were not completely deuterated.

The ATR-FTIR spectra of the unphosphorylated TsDHNS showed peak maxima located between 1640 and 1645  $\text{cm}^{-1}$  (Figure 5). These peaks shifted to 1650–1652  $\text{cm}^{-1}$  for the phosphorylated TsDHNS, indicating a transition from random coil structure to  $\alpha$ -helical structures upon phosphorylation. The band between 1700 and 1800  $\text{cm}^{-1}$  arises because of the free and H-bonded C=O group from lipid molecules. This band has a significantly higher intensity in the case of phosphorylated

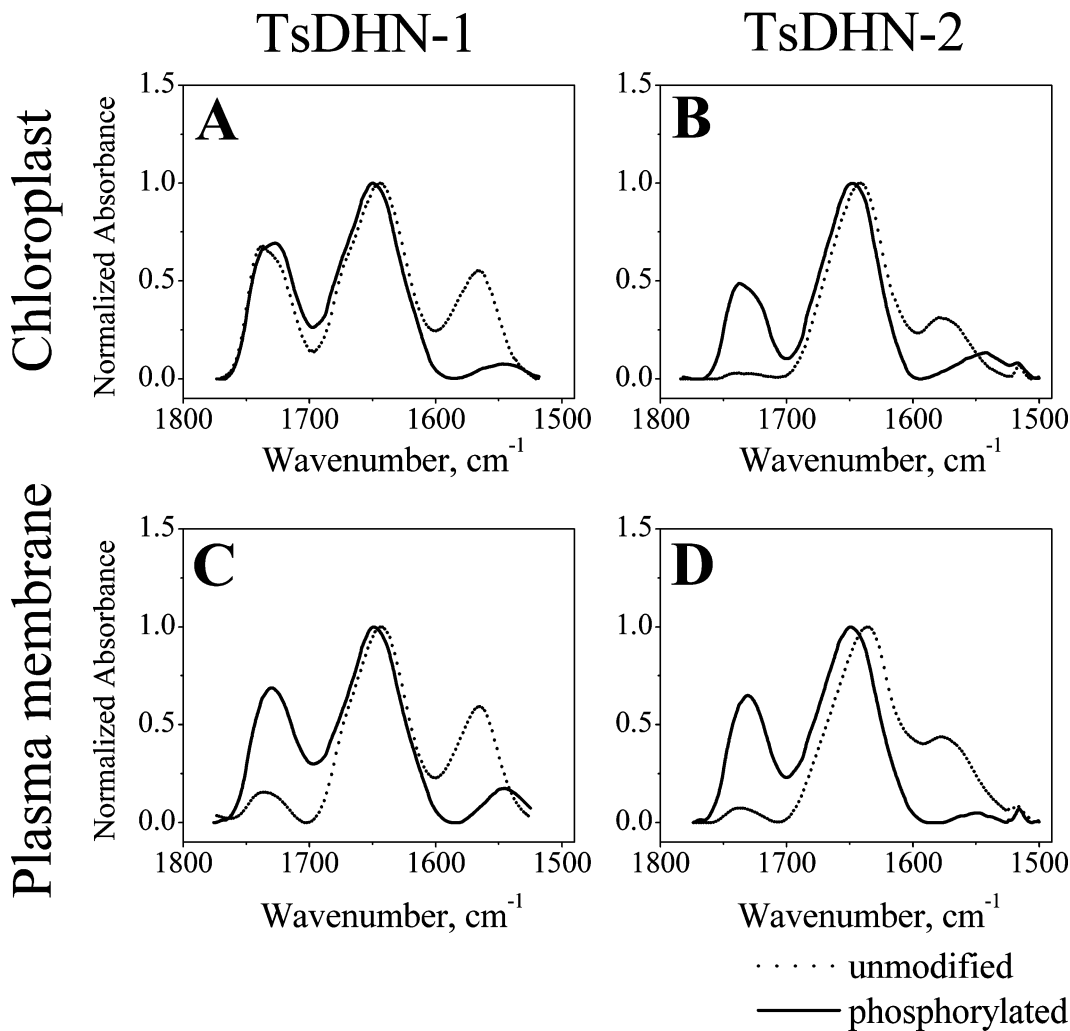


**Figure 5.** Effects of phosphorylation of TsDHN-1 (right) and TsDHN-2 (left), reconstituted with LUVs, on their ATR-FTIR spectra at room temperature (25 °C). The LUV lipid compositions mimic the plant (A and B) chloroplast or (C and D) plasma membrane. Results are representative of experiments performed in triplicate.

TsDHN-1 and TsDHN-2, suggesting a stronger membrane adhering ability of the phosphorylated proteins.

Detailed spectral analysis showed that both TsDHN-1 and TsDHN-2, when bound to lipids, gained more ordered secondary structure upon phosphorylation. The size of the random coil component was reduced noticeably for chloroplast and plasma membrane LUV-associated Phos-TsDHN-1, with the formation of mainly  $\alpha$ -helices and  $\beta$ -sheets to a lesser extent (Tables S1 and S3 of the Supporting Information and Figure 6A–D). For phosphorylated TsDHN-1, the changes were not so dramatic (Tables S2 and S4 of the Supporting Information and Figure 6E–H). For both unmodified and phosphorylated TsDHNs in membrane-associated form, some additional ordered secondary structure was promoted in the presence of Zn<sup>2+</sup>, consistent with our previous study of the unmodified proteins.<sup>9</sup>

**The Degree of Actin Polymerization Is Affected by Phosphorylation of TsDHNs in Vitro.** Apart from a report of a dehydrin–actin interaction observed in transfected fibroblasts,<sup>16</sup> the idea of dehydrins stabilizing cytoskeletal organization in plant cells being subjected to environmental stress has received little attention, to the best of our knowledge. Because IDPs are multifunctional and polymorphic, we have

hypothesized that one or the other of the TsDHN proteins would facilitate actin assembly much in the way that other IDPs such as myelin basic protein do,<sup>56,62</sup> and that post-translational modifications such as phosphorylation and/or environmental conditions such as temperature or the presence of divalent cations can modulate this interaction.

Here, the polymerization of G-actin in the absence and presence of F-buffer, or of unphosphorylated or phosphorylated TsDHNs at an actin:TsDHNs molar ratio of 1:3.2, was followed by measuring the change in the fluorescence intensity of pyrene-labeled actin at 410 nm. A striking difference was observed between the unphosphorylated and phosphorylated TsDHNs in the rate of actin polymerization (Figure 7A). In the presence of unphosphorylated TsDHNs, the emission fluorescence intensity at 410 nm did not change with time. However, in the presence of phosphorylated TsDHNs, the emission fluorescence intensity at 410 nm increased with time, reaching equilibrium within 25 min. The increase in the emission fluorescence intensity was more significant in the case of phosphorylated TsDHN-2. It is evident from this assay that both phosphorylated TsDHNs can polymerize actin in vitro at pH 7.3, whereas unphosphorylated TsDHNs have no effect on G-actin polymerization. Examination of the final state of the

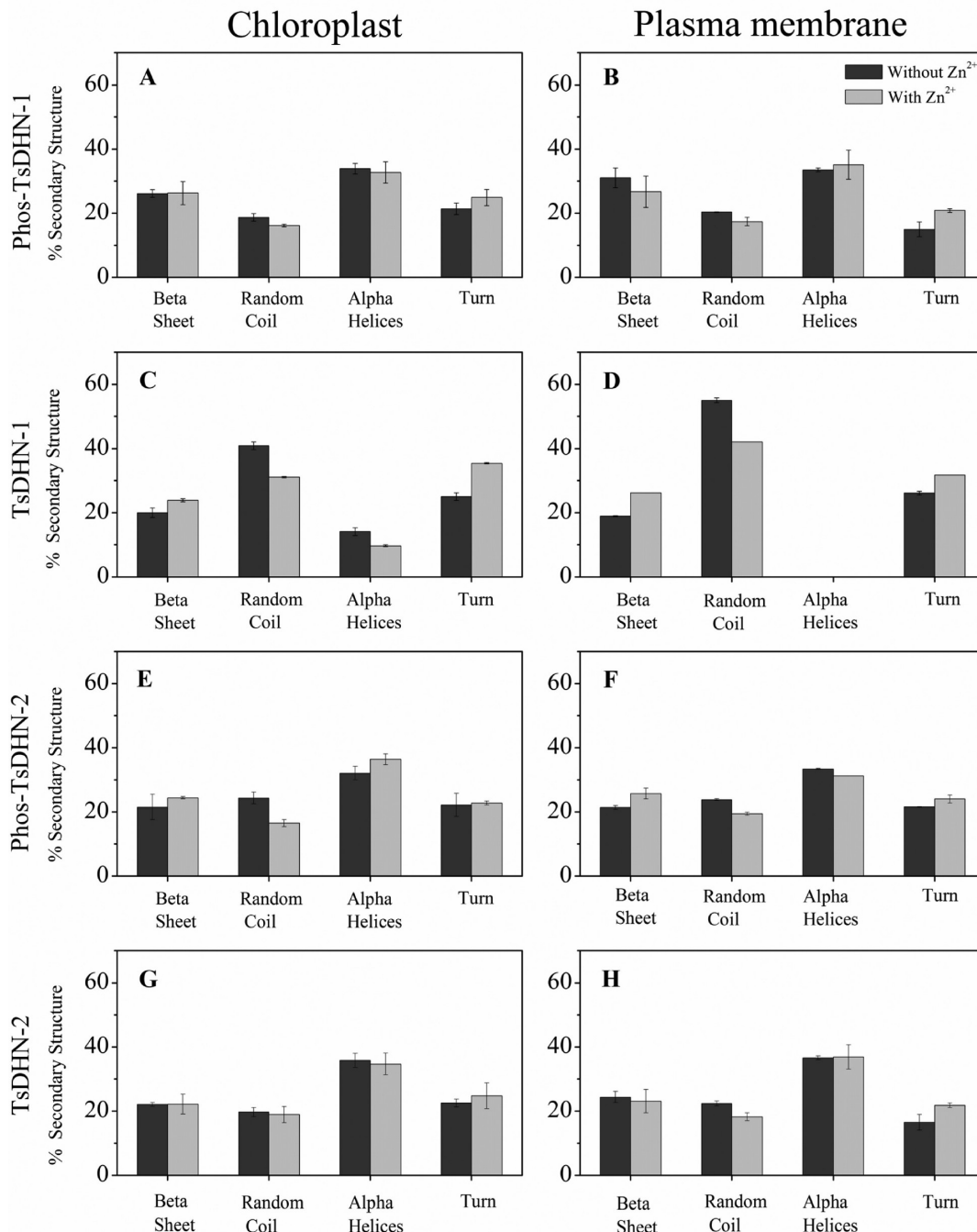


**Figure 6.** Effect of Zn<sup>2+</sup> on the proportion of secondary structure types of membrane-associated (A and B) phosphorylated TsDHN-1, (C and D) unphosphorylated TsDHN-1, (E and F) phosphorylated TsDHN-2, and (G and H) unphosphorylated TsDHN-2, at room temperature (25 °C). The LUV lipid compositions mimic those of the plant (A, C, E, and G) chloroplast or (B, D, F, and H) plasma membranes. Error bars represent the standard deviation of triplicate measurements. Note that the remainder of the structure (to 100%) is contributed by the side chains.

polymerization reaction by transmission electron microscopy revealed that only the phosphorylated TsDHNs cross-linked and bundled actin (Figure 7D,E,G,H). Larger microfilament bundles were observed at a lower actin:TsDHN molar ratio of 1:3.8 (Figure 7F,J).

The bundling of G-actin by the phosphorylated TsDHNs was confirmed by atomic force microscopy. Bundles with diameters ranging from 25 to 55 nm were observed (Figure 8A,E) in the presence of phosphorylated TsDHN-1 at a 1:3.2 actin:TsDHN-2 molar ratio. Actin bundles became more organized (Figure 8B,F) at a lower actin:TsDHN-1 molar

ratio of 1:3.8. Actin bundles with diameters ranging from 30 to 70 nm were observed (Figure 8C,G) in the presence of phosphorylated TsDHN-2 at a 1:3.2 actin:TsDHN-2 molar ratio. Larger actin bundles (Figure 8D,H) were observed at a 1:3.8 actin:TsDHN-2 molar ratio. In the case of salt-induced actin polymerization (F-buffer), the diameters of the actin bundles were within 50–70 nm (Figure 8K). The G-actin alone is shown as a negative control (Figure 8L). Actin bundling was not observed in the presence of unphosphorylated TsDHN-1 (Figure 8I) or TsDHN-2 (Figure 8J).

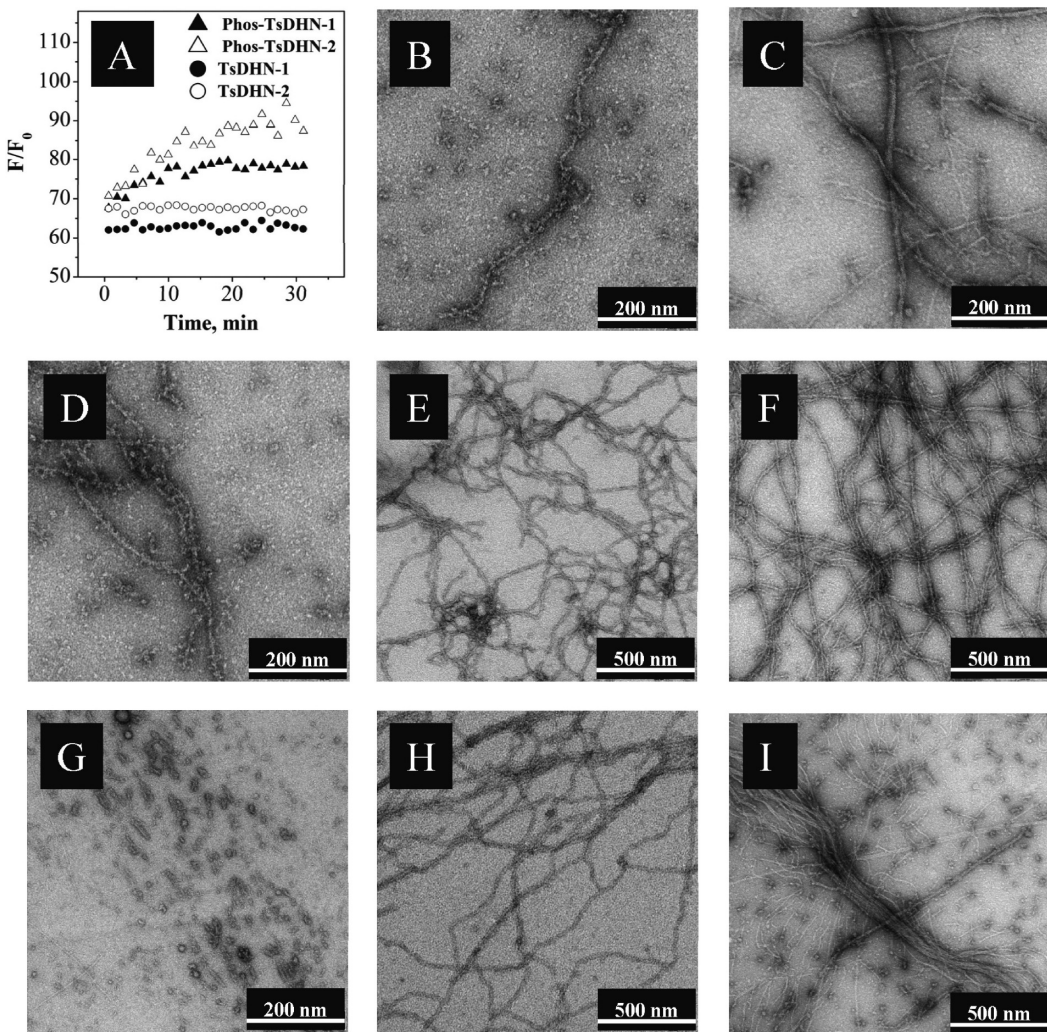


**Figure 7.** Polymerization of actin by the phosphorylated dehydrins TsDHN-1 and TsDHN-2 from *T. salsuginea*. (A) Polymerization of pyrene-labeled G-actin into F-actin bundles induced by unphosphorylated and phosphorylated TsDHNS over time, as a function of the change in emission fluorescence intensity. (B and C) Electron micrographs of G-actin incubated with (B) G-buffer and (C) F-buffer are shown as negative and positive controls, respectively. (D–I) Electron micrographs of G-actin incubated with (D and G) unphosphorylated TsDHNs or (E, F, H, and I) phosphorylated TsDHNs. Specific actin:dehydrin molar ratios are as follows: (D) 1:3.2 actin:unmodified TsDHN-1, (E) 1:3.2 actin:phosphorylated TsDHN-1, (F) 1:3.8 actin:phosphorylated TsDHN-1, (G) 1:3.2 actin:unmodified TsDHN-2, (H) 1:3.2 actin:phosphorylated TsDHN-2, and (I) 1:3.8 actin:phosphorylated TsDHN-2.

**Actin Bundling and Actin–TsDHN Binding.** The strength of the actin–TsDHN interaction and its potential to induce actin bundling were further assessed by a sedimentation assay, in which centrifugation of the polymerization reaction mixture at a low speed allowed only bundled actin to precipitate. The distributions of the proteins were assessed by SDS–PAGE analysis of the supernatant and the pellets. It is shown in Figure 9 that both unmodified TsDHN-1 (Figure 9A, lane 2) and unmodified TsDHN-2 (Figure 9B, lane 2) remained in the supernatants. Actin also remained in the supernatants in both cases, indicating that actin was still in the monomeric form (G-actin). Thus, the unmodified TsDHNS did not induce assembly of G-actin, consistent with the fluorescence data (Figure 7A) and acting as a negative control.

In the case of phosphorylated TsDHN-1 and TsDHN-2, both were found along with actin in the isolated pellets (Figure 9A, lane 5; Figure 9B, lane 5), suggesting that phosphorylated TsDHNS induce bundling of actin and remain bound to the filaments. Although no band (Figure 9A, lane 4) for actin in the

supernatant was observed in the case of phosphorylated TsDHN-1, a strong band (Figure 9B, lane 4) was observed in the case of phosphorylated TsDHN-2, indicating that phosphorylated TsDHN-1 was more efficient in bundling actin.

To assess the interaction between the TsDHNS and G-actin, a high-speed centrifugation assay was performed, in which F-actin (unbundled and bundled) would sediment to the bottom of the tube. These results showed that unmodified TsDHN-2 also interacts with G-actin, presumably to form amorphous assemblies (Figure 9D, lane 3), even though it does not polymerize G-actin as assessed by a pyrene fluorescence assay (Figure 7A). To a lesser extent, this same interaction occurs for unmodified TsDHN-1 (Figure 9C, lane 3).

**Effect of Unphosphorylated TsDHNS on Prepolymerized Actin.** To determine if unphosphorylated dehydrins had an effect on actin assemblies that had previously been polymerized by the phosphorylated form, a variation of the fluorescence polymerization assay was performed. First, phosphorylated TsDHN-1 or TsDHN-2 was added to G-

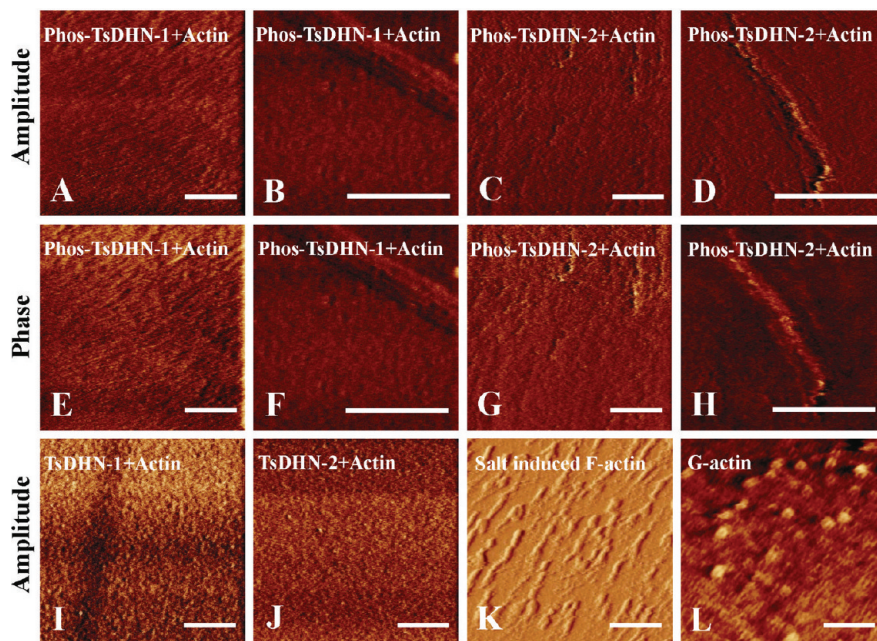


**Figure 8.** Morphology of actin assembly in the presence of unphosphorylated and phosphorylated TsDHNs observed by atomic force microscopy. G-Actin was allowed to interact with TsDHNs under the environmental conditions described in the legend of Figure 7. (A and E) Phosphorylated TsDHN-1 and actin at a 1:3.2 actin:phosphorylated TsDHN-1 molar ratio. (B and F) Phosphorylated TsDHN-1 and actin at a 1:3.8 actin:phosphorylated TsDHN-1 molar ratio. (C and G) Phosphorylated TsDHN-2 and actin at a 1:3.2 actin:phosphorylated TsDHN-2 molar ratio. (D and H) Phosphorylated TsDHN-2 and actin at a 1:3.8 actin:phosphorylated TsDHN-2 molar ratio. (I) Unmodified TsDHN-1 and actin at a 1:3.2 actin:unmodified TsDHN-1 molar ratio. (J) Unmodified TsDHN-2 and actin at a 1:3.2 actin:unmodified TsDHN-2 molar ratio. (K) Salt-induced F-actin. (L) G-actin alone. The scale bars represent 500 nm in each panel.

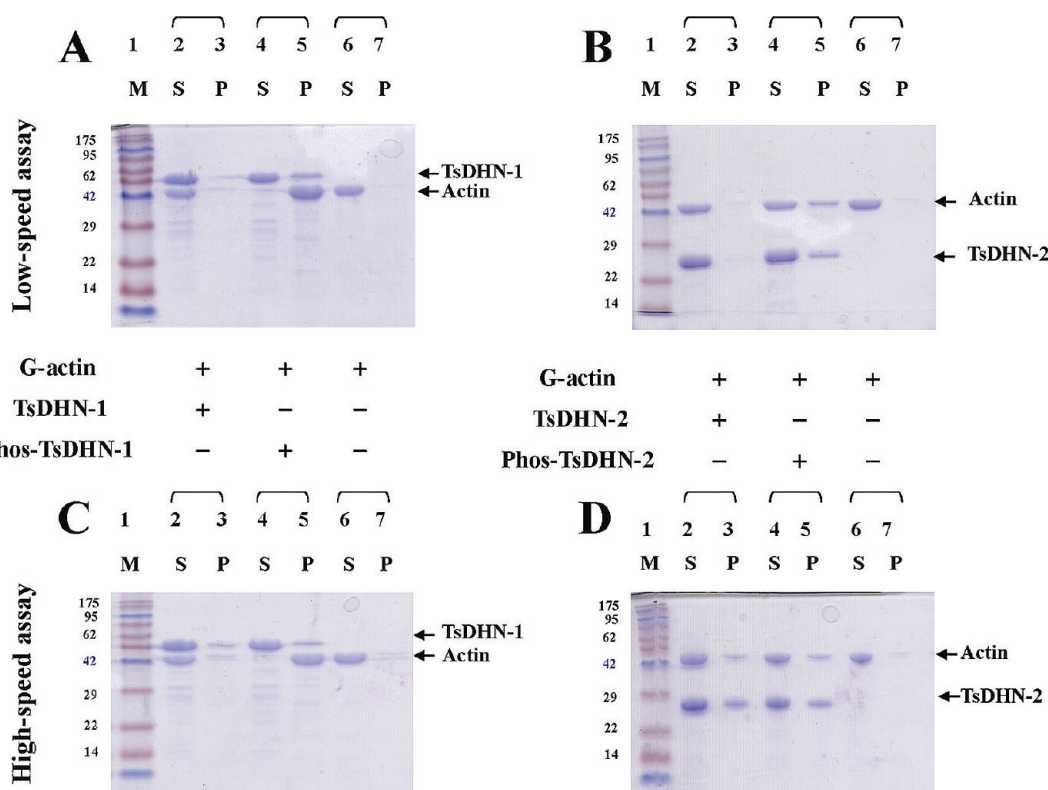


**Figure 9.** Low-speed (A and B) and high-speed (C and D) cosedimentation assay of actin in the presence of unphosphorylated and phosphorylated TsDHN-1 and TsDHN-2. Unphosphorylated or phosphorylated TsDHNs were incubated with G-actin in a 3.6:1 molar ratio at 27 °C in G-buffer and then centrifuged (18000g for low-speed and 100000g for high-speed centrifugation at room temperature for 2 h). Actin alone was used as the negative control. The supernatants and pellets were resuspended in sample buffer as described in Materials and Methods and electrophoresed on 14% SDS-PAGE gels.

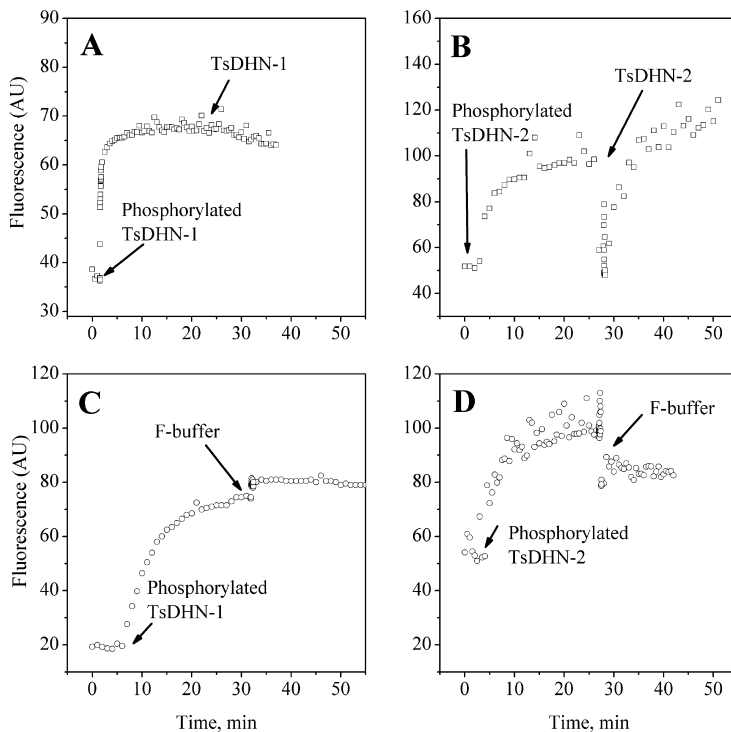


**Figure 10.** Effect of (A) unmodified TsDHN-1 or (B) unmodified TsDHN-2 on actin that had been prepolymerized by phosphorylated TsDHN-1 or TsDHN-2, respectively, studied by measuring the change in fluorescence intensity. (C and D) Effect of F-buffer on actin that had been prepolymerized by phosphorylated TsDHN-1 and TsDHN-2, respectively, studied by measuring the change in fluorescence intensity. Results are representative of experiments performed in triplicate.

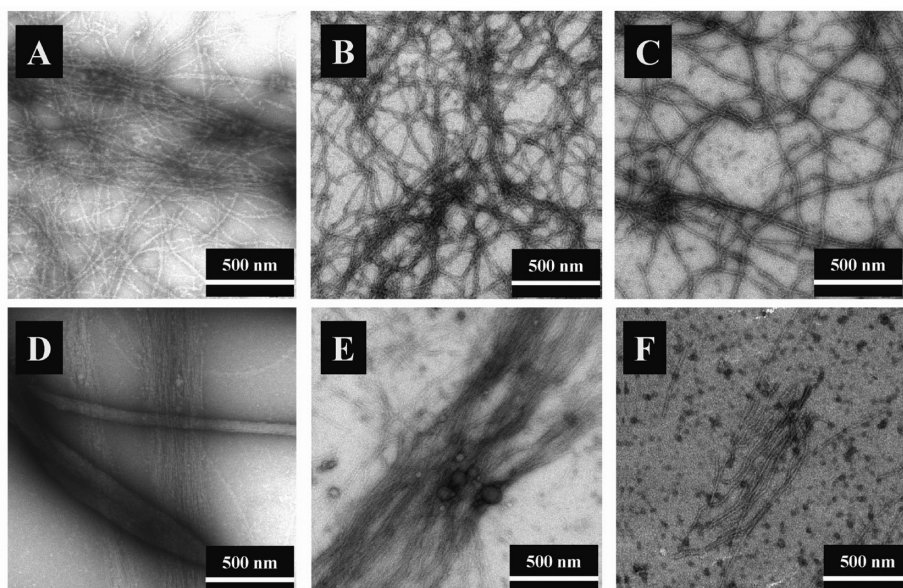


**Figure 11.** Effect of unmodified TsDHN on prepolymerized F-actin. (A–F) Electron micrographs of (A and B) Phos-TsDHN-1-polymerized G-actin incubated with unphosphorylated TsDHN-1 at actin:Phos-TsDHN:TsDHN molar ratios of 1:3:3 (A) and 1:4:3 (B), (C) Phos-TsDHN-1-polymerized G-actin incubated with F-buffer, (D and E) Phos-TsDHN-2-polymerized G-actin incubated with unphosphorylated TsDHN-2 at actin:Phos-TsDHN:TsDHN molar ratios of 1:3:3 (D) and 1:4:3 (E), and (F) TsDHN-2 polymerized G-actin incubated with F-buffer.

actin at a 1:3.0 or 1:4:0 molar ratio, and this mixture was incubated for roughly 25 min to effect actin polymerization to proceed to its maximal level. Then, the corresponding unmodified form was added to achieve a final actin:Phos-TsDHN:TsDHN molar ratio of 1:3:3 or 1:4:3. The results are compiled in Figure 10. Addition of unphosphorylated TsDHN-1 had no influence on the fluorescence intensity of the actin

polymerized to its maximum level by phosphorylated TsDHN-1 (Figure 10A). However, the addition of unphosphorylated TsDHN-2 to F-actin increased the fluorescence intensity further (Figure 10B), probably because of its ability to bind actin even in the unmodified form (Figure 9D, lane 3). This binding could produce more ordered actin bundles and, therefore, cause an additional increase in fluorescence intensity.

The F-buffer alone had no effect on the prepolymerized actin (Figure 10C,D).

The observed morphologies of the actin assemblies studied by transmission electron microscopy support the results obtained by fluorescence measurements (Figure 11). No change in the morphology of the actin assemblies induced by phosphorylated TsDHN-1 was observed with the addition of unphosphorylated TsDHN-1 (Figure 11A,B). More organized actin sheets were observed when unmodified TsDHN-2 was added to the actin assemblies induced by phosphorylated TsDHN-2 (Figure 11D,E), thus supporting the results presented in Figure 10B. No change in the morphology of the actin assemblies induced by any of the phosphorylated TsDHNs was observed when F-buffer alone was added to the assemblies (Figure 11C,F).

## ■ DISCUSSION

Intrinsically disordered proteins are generally highly modified, especially by phosphorylation,<sup>63</sup> and are multifunctional, with multiple interacting partners and diverse disorder-to-order transitions.<sup>64,65</sup> The conformations of IDPs in general are dynamic and highly dependent on environmental conditions such as temperature, pH, and salt concentrations<sup>66</sup> faced by plants being subjected to abiotic stress,<sup>67</sup> as has been recognized for dehydrins in particular.<sup>20,68</sup> Such considerations have motivated us to investigate further potential physiological roles of TsDHN-1 and TsDHN-2 in maintaining the drought and cold tolerance of *T. salsuginea*.<sup>8,9</sup> Here specifically, we have examined the effects of phosphorylation and divalent cations on the secondary structure of these dehydrins, because regular secondary structure elements induced in this way during the abiotic stress response may represent preformed recognition elements for binding other proteins.<sup>64,65</sup> Moreover, we have investigated a new potential function of dehydrins in stabilizing the actin cytoskeleton of plant cells being subjected to environmental stress.

Our results show that neither the acidic TsDHN-1 nor the basic TsDHN-2 alone gains any ordered secondary structure upon phosphorylation except when associated with LUVs. This observation is in agreement with previous work in which it was shown that phosphorylated and unphosphorylated COR47 have similar secondary structure compositions.<sup>20</sup> The  $\alpha$ -helical component of the secondary structure in the phosphorylated COR47 is promoted in the presence of 50% glycerine. Other macromolecules such as sucrose or glucose did not cause any significant change in secondary structure in phosphorylated COR47. Here, in particular, both the acidic and basic phosphorylated *T. salsuginea* dehydrins gain PPII structure with a decrease in temperature. Hallmarks of IDPs are their association with multiple binding partners, often with concomitant disorder-to-order transitions of the binding segments.<sup>64,65</sup> Because the PPII conformation is an important component of IDPs in general<sup>39,56</sup> and is required for specific associations such as those with SH3 domains,<sup>56</sup> the observations here of induced PPII conformations in *T. salsuginea* dehydrins, and elsewhere in other dehydrin species,<sup>57</sup> support the scenario of dehydrin multifunctionality in maintaining plant cell stress response. We thus suggest here that the phosphorylated TsDHN variants interact with other ligand molecules through the PPII at low temperatures. We have also shown here by ATR-FTIR spectroscopy that phosphorylated TsDHN-1 and TsDHN-2 undergo disorder-

to-order transitions upon binding to LUVs and that they interact with and polymerize G-actin.

Other intrinsically disordered proteins are also known to regulate actin polymerization. It has been shown in previous studies that classic 18.5 kDa myelin basic protein (MBP), and the microtubule assembly protein tau via its proline-rich domain, were able to polymerize, bundle, and link actin to phospholipid membranes.<sup>62,69</sup> Post-translational modifications such as phosphorylation or deimination of MBP, or phosphorylation of tau, are known to enhance the ability of these proteins to polymerize G-actin.<sup>62,69</sup> Here, we have shown that phosphorylation of *T. salsuginea* dehydrins allows them to polymerize actin in vitro, which supports future study of this phenomenon in vivo. There are examples of physiologically significant phosphorylation-regulated actin polymerization by other plant proteins.<sup>70–72</sup> Phosphorylation of the protein TaADF, the wheat (*Triticum aestivum*) actin depolymerization factor, has been shown to decrease the rate of depolymerization of F-actin and increase the stability of F-actin.<sup>73</sup> Stabilization of F-actin may, in turn, contribute to membrane stabilization in plants being subjected to stress.<sup>74</sup>

Actin polymerization in plants is also regulated by pH as seen in animals. Proteins containing the LIM domain (double-zinc finger motif, named after its initial discovery in the proteins Lin11, Isl-1, and Mec-3) are known to interact with actin in animal and plant cells in a pH-dependent manner. It has been shown that a widely expressed LIM domain-containing plant protein, WLIM, is able to polymerize G-actin regardless of pH, but a pollen-specific protein PLIM is able to polymerize actin only at a lower pH (6.9).<sup>75,76</sup> In this study, we have shown that TsDHN-1 and TsDHN-2 are able to polymerize G-actin and bundle F-actin at pH 7.3 only upon being phosphorylated.

Actin dynamics may have a role in protecting plant cells during low-temperature stress. Actin-reorganizing factors such as ADFs and elongation factor-1 are upregulated<sup>77–79</sup> in acclimated plant cells by low temperatures. It is also known that the proportion of phosphorylated dehydrins is elevated at low temperatures in cold-acclimated plants.<sup>73</sup> Depolymerization of actin by ADFs may prevent expansion-induced cell lysis during freeze-thaw cycles. In more extreme situations, programmed cell death initiated in response to environmental stress involves actin polymerization-depolymerization dynamics and may be induced by Ca<sup>2+</sup> signaling.<sup>80–83</sup> Actin depolymerization causes elevation of the intracellular Ca<sup>2+</sup> concentration in the olive tree, and this increase is enhanced during cold stress.<sup>84</sup> The involvement of dehydrins in such cytoskeletal remodeling events is worthy of further study. Moreover, there are many examples of mammalian proteins that are CKII substrates whose nuclear localization has been proposed to be regulated by phosphorylation,<sup>32</sup> and it would be of interest to investigate potential intracellular trafficking of phosphorylated dehydrins in plant cells being subjected to abiotic stress.

In summary, we have shown here that various environmentally induced conditions such as changes in intracellular pH and cation concentration, as well as phosphorylation, regulate the folding of TsDHN-1 and TsDHN-2 with or without their association with a membrane. Calcium induces a PPII conformation in phosphorylated TsDHN-2, which may aid it in polymerizing G-actin. The TsDHN conformations and activities modulated by phosphorylation, cation binding, and temperature and pH changes appear to play an important role in regulating actin polymerization dynamics. Taken together, our results support the hypothesis that dehydrins may also play

a role in stabilizing the cytoskeleton of *T. salsuginea* cells being subjected to periods of extreme drought and cold stress.

## ASSOCIATED CONTENT

### Supporting Information

Figures S1–S3 and Tables S1–S4. This material is available free of charge via the Internet at <http://pubs.acs.org>.

## AUTHOR INFORMATION

### Corresponding Author

\*Department of Molecular and Cellular Biology, University of Guelph, 50 Stone Rd. E., Guelph, Ontario N1G 2W1, Canada. Phone: (519) 824-4120, ext. 52535. Fax: (519) 837-1802. E-mail: gharauz@uoguelph.ca

### Funding

This work was supported by a Discovery Grant from the Natural Sciences and Engineering Research Council of Canada (RG121541 to G.H.). G.S.T.S. and V.V.B. are recipients of a Doctoral Studentship and a Postdoctoral Fellowship, respectively, from the Multiple Sclerosis Society of Canada. J.R.D. acknowledges support from the Canada Research Chairs Program.

## ACKNOWLEDGMENTS

The pET28b plasmid encoding recombinant SUMO protease, His-tagged Ulp(403–621), was a kind gift from Dr. Christopher Lima (Sloan-Kettering Institute). We are grateful to Mr. Robert Harris for assistance with the electron microscopy, to Dr. Frances Sharom for use of her Zetasizer instrument, and to Dr. Leonid Brown for helpful comments on the manuscript.

## ABBREVIATIONS

ADF, actin depolymerization factor; ATR, attenuated total reflection; CD, circular dichroism; Chol, cholesterol; CKII, casein kinase II; DMPC, dimyristoylphosphatidylglycerol; ESI, electrospray ionization; FTIR, Fourier transform infrared; IDP, intrinsically disordered protein; LEA, late embryogenesis abundant; MGDG, monogalactosyldiacylglycerol; PBS, phosphate-buffered saline; PC, phosphatidylcholine; PCR, polymerase chain reaction; PE, phosphatidylethanolamine; PI, phosphatidylinositol; PPII, polyproline type II conformation; PS, phosphatidylserine; SQDG, sulfoquinovosyl diacylglycerol; TsDHN-1, acidic *T. salsuginea* dehydrin 1; TsDHN-2, basic *T. salsuginea* dehydrin 2.

## REFERENCES

- Battaglia, M., Olvera-Carrillo, Y., Garciarrubio, A., Campos, F., and Covarrubias, A. A. (2008) The enigmatic LEA proteins and other hydrophilins. *Plant Physiol.* 148, 6–24.
- Hundertmark, M., and Hincha, D. K. (2008) LEA (late embryogenesis abundant) proteins and their encoding genes in *Arabidopsis thaliana*. *BMC Genomics* 9, 118.
- Close, T. J. (1997) Dehydrins: A commonality in the response of plants to dehydration and low temperature. *Physiol. Plant.* 100, 291–296.
- Kosova, K., Vitamvas, P., and Prasil, I. T. (2007) The role of dehydrins in plant response to cold. *Biol. Plant.* 51, 601–617.
- Tommasini, L., Svensson, J. T., Rodriguez, E. M., Wahid, A., Malatrasi, M., Kato, K., Wanamaker, S., Resnik, J., and Close, T. J. (2008) Dehydrin gene expression provides an indicator of low temperature and drought stress: Transcriptome-based analysis of barley (*Hordeum vulgare* L.). *Funct. Integr. Genomics* 8, 387–405.
- Eriksson, S. K., and Harryson, P. (2011) Dehydrins: Molecular biology, structure, and function. In *Plant Desiccation Tolerance* (Lüttge, U., Ed.) pp 289–304, Springer-Verlag, Berlin.
- Tunnacliffe, A., and Wise, M. J. (2007) The continuing conundrum of the LEA proteins. *Naturwissenschaften* 94, 791–812.
- Rahman, L. N., Chen, L., Nazim, S., Bamm, V. V., Yaish, M. W., Moffatt, B. A., Dutcher, J. R., and Harauz, G. (2010) Interactions of intrinsically disordered *Thellungiella salsuginea* dehydrins TsDHN-1 and TsDHN-2 with membranes: Synergistic effects of lipid composition and temperature on secondary structure. *Biochem. Cell Biol.* 88, 791–807.
- Rahman, L. N., Bamm, V. V., Voyer, J. A. M., Smith, G. S., Chen, L., Yaish, M. W., Moffatt, B. A., Dutcher, J. R., and Harauz, G. (2011) Zinc induces disorder-to-order transitions in free and membrane-associated *Thellungiella salsuginea* dehydrins TsDHN-1 and TsDHN-2: A solution CD and solid-state ATR-FTIR study. *Amino Acids* 40, 1485–1502.
- Haaning, S., Radutoiu, S., Hoffmann, S. V., Dittmer, J., Giehm, L., Otzen, D. E., and Stougaard, J. (2008) An unusual intrinsically disordered protein from the model legume *Lotus japonicus* stabilizes proteins *in vitro*. *J. Biol. Chem.* 283, 31142–31152.
- Kovacs, D., Kalmar, E., Torok, Z., and Tompa, P. (2008) Chaperone activity of ERD10 and ERD14, two disordered stress-related plant proteins. *Plant Physiol.* 147, 381–390.
- Tompa, P., and Kovacs, D. (2010) Intrinsically disordered chaperones in plants and animals. *Biochem. Cell Biol.* 88, 167–174.
- Hughes, S., and Graether, S. P. (2011) Cryoprotective mechanism of a small intrinsically disordered dehydrin protein. *Protein Sci.* 20, 42–50.
- Hundertmark, M., Dimova, R., Lengfeld, J., Seckler, R., and Hincha, D. K. (2011) The intrinsically disordered late embryogenesis abundant protein LEA18 from *Arabidopsis thaliana* modulates membrane stability through binding and folding. *Biochim. Biophys. Acta* 1808, 446–453.
- Eriksson, S. K., Kutzer, M., Procek, J., Grobner, G., and Harryson, P. (2011) Tunable membrane binding of the intrinsically disordered dehydrin Iti30, a cold-induced plant stress protein. *Plant Cell* 23, 2391–2404.
- Abu-Abied, M., Golomb, L., Belausov, E., Huang, S., Geiger, B., Kam, Z., Staiger, C. J., and Sadot, E. (2006) Identification of plant cytoskeleton-interacting proteins by screening for actin stress fiber association in mammalian fibroblasts. *Plant J.* 48, 367–379.
- Battaglia, M., Solorzano, R. M., Hernandez, M., Cuellar-Ortiz, S., Garcia-Gomez, B., Marquez, J., and Covarrubias, A. A. (2007) Proline-rich cell wall proteins accumulate in growing regions and phloem tissue in response to water deficit in common bean seedlings. *Planta* 225, 1121–1133.
- Hara, M., Shinoda, Y., Tanaka, Y., and Kuboi, T. (2009) DNA binding of *Citrus* dehydrin promoted by zinc ion. *Plant Cell Environ.* 32, 532–541.
- Receveur-Bréchet, V., Bourhis, J. M., Uversky, V. N., Canard, B., and Longhi, S. (2006) Assessing protein disorder and induced folding. *Proteins* 62, 24–45.
- Mouillon, J. M., Eriksson, S. K., and Harryson, P. (2008) Mimicking the plant-cell interior under water stress by macromolecular crowding: Disordered dehydrin proteins are highly resistant to structural collapse. *Plant Physiol.* 148, 1925–1937.
- Tompa, P., Banki, P., Bokor, M., Kamasa, P., Kovacs, D., Lasanda, G., and Tompa, K. (2006) Protein-water and protein-buffer interactions in the aqueous solution of an intrinsically unstructured plant dehydrin: NMR intensity and DSC aspects. *Biophys. J.* 91, 2243–2249.
- Heyen, B. J., Alsheikh, M. K., Smith, E. A., Torvik, C. F., Seals, D. F., and Randall, S. K. (2002) The calcium-binding activity of a vacuole-associated, dehydrin-like protein is regulated by phosphorylation. *Plant Physiol.* 130, 675–687.
- Alsheikh, M. K., Heyen, B. J., and Randall, S. K. (2003) Ion binding properties of the dehydrin ERD14 are dependent upon phosphorylation. *J. Biol. Chem.* 278, 40882–40889.

- (24) Hara, M., Fujinaga, M., and Kuboi, T. (2004) Radical scavenging activity and oxidative modification of *Citrus* dehydrin. *Plant Physiol. Biochem.* 42, 657–662.
- (25) Hara, M., Fujinaga, M., and Kuboi, T. (2005) Metal binding by citrus dehydrin with histidine-rich domains. *J. Exp. Bot.* 56, 2695–2703.
- (26) Rom, S., Gilad, A., Kalifa, Y., Konrad, Z., Karpasas, M. M., Goldgur, Y., and Bar-Zvi, D. (2006) Mapping the DNA- and zinc-binding domains of ASR1 (abscisic acid stress ripening), an abiotic-stress regulated plant specific protein. *Biochimie* 88, 621–628.
- (27) Goldgur, Y., Rom, S., Ghirlando, R., Shkolnik, D., Shadrin, N., Konrad, Z., and Bar-Zvi, D. (2007) Desiccation and zinc binding induce transition of tomato abscisic acid stress ripening 1, a water stress- and salt stress-regulated plant-specific protein, from unfolded to folded state. *Plant Physiol.* 143, 617–628.
- (28) Xu, J., Zhang, Y. X., Wei, W., Han, L., Guan, Z. Q., Wang, Z., and Chai, T. Y. (2008) BjDHNs confer heavy-metal tolerance in plants. *Mol. Biotechnol.* 38, 91–98.
- (29) Mu, P., Feng, D., Su, J., Zhang, Y., Dai, J., Jin, H., Liu, B., He, Y., Qi, K., Wang, H., and Wang, J. (2011) Cu<sup>2+</sup> triggers reversible aggregation of a disordered His-rich dehydrin MpDhn12 from *Musa paradisiaca*. *J. Biochem.*, DOI: doi: 10.1093/jb/mvr082.
- (30) Mehta, P. A., Rebala, K. C., Venkataraman, G., and Parida, A. (2009) A diurnally regulated dehydrin from *Avicennia marina* that shows nucleo-cytoplasmic localization and is phosphorylated by casein kinase II *in vitro*. *Plant Physiol. Biochem.* 47, 701–709.
- (31) Jiang, X., and Wang, Y. (2004) β-Elimination coupled with tandem mass spectrometry for the identification of *in vivo* and *in vitro* phosphorylation sites in maize dehydrin DHN1 protein. *Biochemistry* 43, 15567–15576.
- (32) Nardozzi, J. D., Lott, K., and Cingolani, G. (2010) Phosphorylation meets nuclear import: A review. *Cell Commun. Signaling* 8, 32.
- (33) Plotnikov, A., Zehorai, E., Procaccia, S., and Seger, R. (2011) The MAPK cascades: Signaling components, nuclear roles and mechanisms of nuclear translocation. *Biochim. Biophys. Acta* 1813, 1619–1633.
- (34) Jensen, A. B., Goday, A., Figueras, M., Jessop, A. C., and Pages, M. (1998) Phosphorylation mediates the nuclear targeting of the maize Rab17 protein. *Plant J.* 13, 691–697.
- (35) Vilardell, J., Goday, A., Freire, M. A., Torrent, M., Martinez, M. C., Torne, J. M., and Pages, M. (1990) Gene sequence, developmental expression, and protein phosphorylation of RAB-17 in maize. *Plant Mol. Biol.* 14, 423–432.
- (36) Wong, C. E., Li, Y., Whitty, B. R., Diaz-Camino, C., Akhter, S. R., Brandle, J. E., Golding, G. B., Weretilnyk, E. A., Moffatt, B. A., and Griffith, M. (2005) Expressed sequence tags from the Yukon ecotype of *Thellungiella* reveal that gene expression in response to cold, drought and salinity shows little overlap. *Plant Mol. Biol.* 58, 561–574.
- (37) Griffith, M., Timonin, M., Wong, A. C., Gray, G. R., Akhter, S. R., Saldanha, M., Rogers, M. A., Weretilnyk, E. A., and Moffatt, B. (2007) *Thellungiella*: An *Arabidopsis*-related model plant adapted to cold temperatures. *Plant Cell Environ.* 30, 529–538.
- (38) Amtmann, A. (2009) Learning from evolution: *Thellungiella* generates new knowledge on essential and critical components of abiotic stress tolerance in plants. *Mol. Plant* 2, 3–12.
- (39) Rath, A., Davidson, A. R., and Deber, C. M. (2005) The structure of “unstructured” regions in peptides and proteins: Role of the polyproline II helix in protein folding and recognition. *Biopolymers* 80, 179–185.
- (40) Mossessova, E., and Lima, C. D. (2000) Ulp1-SUMO crystal structure and genetic analysis reveal conserved interactions and a regulatory element essential for cell growth in yeast. *Mol. Cell* 5, 865–876.
- (41) Jacob, A. M., and Turck, C. W. (2008) Detection of post-translational modifications by fluorescent staining of two-dimensional gels. *Methods Mol. Biol.* 446, 21–32.
- (42) Yan, J. X., Harry, R. A., Spibey, C., and Dunn, M. J. (2000) Postelectrophoretic staining of proteins separated by two-dimensional gel electrophoresis using SYPRO dyes. *Electrophoresis* 21, 3657–3665.
- (43) Bamm, V. V., and Harauz, G. (2008) Expression and purification of the active variant of recombinant murine Golli-interacting protein (GIP): Characterization of its phosphatase activity and interaction with Golli-BG21. *Protein Expression Purif.* 62, 36–43.
- (44) Bamm, V. V., De Avila, M., Smith, G. S., Ahmed, M. A., and Harauz, G. (2011) Structured functional domains of myelin basic protein: Cross talk between actin polymerization and Ca<sup>2+</sup>-dependent calmodulin interaction. *Biophys. J.* 101, 1248–1256.
- (45) Pardee, J. D., and Spudich, J. A. (1982) Purification of muscle actin. *Methods Cell Biol.* 24, 271–289.
- (46) Bamm, V. V., Ahmed, M. A., and Harauz, G. (2010) Interaction of myelin basic protein with actin in the presence of dodecylphosphocholine micelles. *Biochemistry* 49, 6903–6915.
- (47) Ahmed, M. A. M., Bamm, V. V., Shi, L., Steiner-Mosonyi, M., Dawson, J. F., Brown, L., Harauz, G., and Ladizhansky, V. (2009) Induced secondary structure and polymorphism in an intrinsically disordered structural linker of the CNS: Solid-state NMR and FTIR spectroscopy of myelin basic protein bound to actin. *Biophys. J.* 96, 180–191.
- (48) Boggs, J. M., Rangaraj, G., Gao, W., and Heng, Y. M. (2006) Effect of phosphorylation of myelin basic protein by MAPK on its interactions with actin and actin binding to a lipid membrane *in vitro*. *Biochemistry* 45, 391–401.
- (49) Malakhov, M. P., Mattern, M. R., Malakhova, O. A., Drinker, M., Weeks, S. D., and Butt, T. R. (2004) SUMO fusions and SUMO-specific protease for efficient expression and purification of proteins. *J. Struct. Funct. Genomics* 5, 75–86.
- (50) Satakarni, M., and Curtis, R. (2011) Production of recombinant peptides as fusions with SUMO. *Protein Expression Purif.* 78, 113–119.
- (51) Kader, M. A., and Lindberg, S. (2010) Cytosolic calcium and pH signaling in plants under salinity stress. *Plant Signaling Behav.* 5, 233–238.
- (52) Koyama, H., Toda, T., and Hara, T. (2001) Brief exposure to low-pH stress causes irreversible damage to the growing root in *Arabidopsis thaliana*: Pectin-Ca interaction may play an important role in proton rhizotoxicity. *J. Exp. Bot.* 52, 361–368.
- (53) Mathieu, Y., Jouanneau, J. P., Thomine, S., Lapous, D., and Guern, J. (1994) Cytosolic protons as secondary messengers in elicitor-induced defence responses. *Biochem. Soc. Symp.* 60, 113–130.
- (54) Roos, W., Viehweger, K., Dordschbal, B., Schumann, B., Evers, S., Steighardt, J., and Schwartze, W. (2006) Intracellular pH signals in the induction of secondary pathways: The case of *Eschscholzia californica*. *J. Plant Physiol.* 163, 369–381.
- (55) Polverini, E., Rangaraj, G., Libich, D. S., Boggs, J. M., and Harauz, G. (2008) Binding of the proline-rich segment of myelin basic protein to SH3-domains: Spectroscopic, microarray, and modelling studies of ligand conformation and effects of post-translational modifications. *Biochemistry* 47, 267–282.
- (56) Harauz, G., and Libich, D. S. (2009) The classic basic protein of myelin: Conserved structural motifs and the dynamic molecular barcode involved in membrane adhesion and protein-protein interactions. *Curr. Protein Pept. Sci.* 10, 196–215.
- (57) Soulages, J. L., Kim, K., Arrese, E. L., Walters, C., and Cushman, J. C. (2003) Conformation of a group 2 late embryogenesis abundant protein from soybean. Evidence of poly(L-proline)-type II structure. *Plant Physiol.* 131, 963–975.
- (58) Mazars, C., Bourque, S., Mithofer, A., Pugin, A., and Ranjeva, R. (2009) Calcium homeostasis in plant cell nuclei. *New Phytol.* 181, 261–274.
- (59) Reddy, V. S., and Reddy, A. S. (2004) Proteomics of calcium-signaling components in plants. *Phytochemistry* 65, 1745–1776.
- (60) Jung, C. (2000) Insight into protein structure and protein-ligand recognition by Fourier transform infrared spectroscopy. *J. Mol. Recognit.* 13, 325–351.
- (61) Goormaghtigh, E., Gasper, R., Benard, A., Goldsztein, A., and Raussens, V. (2009) Protein secondary structure content in solution,

- films and tissues: Redundancy and complementarity of the information content in circular dichroism, transmission and ATR FTIR spectra. *Biochim. Biophys. Acta* 1794, 1332–1343.
- (62) Harauz, G., Ladizhansky, V., and Boggs, J. M. (2009) Structural polymorphism and multifunctionality of myelin basic protein. *Biochemistry* 48, 8094–8104.
- (63) Iakoucheva, L. M., Radivojac, P., Brown, C. J., O'Connor, T. R., Sikes, J. G., Obradovic, Z., and Dunker, A. K. (2004) The importance of intrinsic disorder for protein phosphorylation. *Nucleic Acids Res.* 32, 1037–1049.
- (64) Vacic, V., Oldfield, C. J., Mohan, A., Radivojac, P., Cortese, M. S., Uversky, V. N., and Dunker, A. K. (2007) Characterization of molecular recognition features, MoRFs, and their binding partners. *J. Proteome Res.* 6, 2351–2366.
- (65) Tompa, P., and Fuxreiter, M. (2008) Fuzzy complexes: Polymorphism and structural disorder in protein-protein interactions. *Trends Biochem. Sci.* 33, 2–8.
- (66) Uversky, V. N. (2009) Intrinsically disordered proteins and their environment: Effects of strong denaturants, temperature, pH, counter ions, membranes, binding partners, osmolytes, and macromolecular crowding. *Protein J.* 28, 305–325.
- (67) Wang, H., Wu, Z., Chen, Y., Yang, C., and Shi, D. (2011) Effects of salt and alkali stresses on growth and ion balance in rice (*Oryza sativa* L.). *Plant Soil Environ.* 57, 286–294.
- (68) Szalaine, A. B., Kovacs, D., Tompa, P., and Perczel, A. (2011) Full backbone assignment and dynamics of the intrinsically disordered dehydrin ERD14. *Biomol. NMR Assignments* 5, 189–193.
- (69) He, H. J., Wang, X. S., Pan, R., Wang, D. L., Liu, M. N., and He, R. Q. (2009) The proline-rich domain of tau plays a role in interactions with actin. *BMC Cell Biol.* 10, 81.
- (70) Volkmann, D., and Baluska, F. (1999) Actin cytoskeleton in plants: From transport networks to signaling networks. *Microsc. Res. Tech.* 47, 135–154.
- (71) Chen, C. Y., Cheung, A. Y., and Wu, H. M. (2003) Actin-depolymerizing factor mediates Rac/Rop GTPase-regulated pollen tube growth. *Plant Cell* 15, 237–249.
- (72) Chen, C. W., Yang, Y. W., Lur, H. S., Tsai, Y. G., and Chang, M. C. (2006) A novel function of abscisic acid in the regulation of rice (*Oryza sativa* L.) root growth and development. *Plant Cell Physiol.* 47, 1–13.
- (73) Ouellet, F., Carpentier, E., Cope, M. J., Monroy, A. F., and Sarhan, F. (2001) Regulation of a wheat actin-depolymerizing factor during cold acclimation. *Plant Physiol.* 125, 360–368.
- (74) Hohenberger, P., Eing, C., Straessner, R., Durst, S., Frey, W., and Nick, P. (2011) Plant actin controls membrane permeability. *Biochim. Biophys. Acta* 1808, 2304–2312.
- (75) Wang, H. J., Wan, A. R., and Jauh, G. Y. (2008) An actin-binding protein, LILIM1, mediates calcium and hydrogen regulation of actin dynamics in pollen tubes. *Plant Physiol.* 147, 1619–1636.
- (76) Papuga, J., Hoffmann, C., Dieterle, M., Moes, D., Moreau, F., Tholl, S., Steinmetz, A., and Thomas, C. (2010) *Arabidopsis* LIM proteins: A family of actin bundlers with distinct expression patterns and modes of regulation. *Plant Cell* 22, 3034–3052.
- (77) Chen, C. Y., Wong, E. I., Vidali, L., Estavillo, A., Hepler, P. K., Wu, H. M., and Cheung, A. Y. (2002) The regulation of actin organization by actin-depolymerizing factor in elongating pollen tubes. *Plant Cell* 14, 2175–2190.
- (78) Dunn, M. A., Morris, A., Jack, P. L., and Hughes, M. A. (1993) A low-temperature-responsive translation elongation factor 1 $\alpha$  from barley (*Hordeum vulgare* L.). *Plant Mol. Biol.* 23, 221–225.
- (79) Thomashow, M. F. (1999) Plant Cold Acclimation: Freezing Tolerance Genes and Regulatory Mechanisms. *Annu. Rev. Plant Physiol. Plant Mol. Biol.* 50, 571–599.
- (80) Reape, T. J., and McCabe, P. F. (2010) Apoptotic-like regulation of programmed cell death in plants. *Apoptosis* 15, 249–256.
- (81) Gourlay, C. W., and Ayscough, K. R. (2005) The actin cytoskeleton: A key regulator of apoptosis and ageing? *Nat. Rev. Mol. Cell Biol.* 6, 583–589.
- (82) Franklin-Tong, V. E., and Gourlay, C. W. (2008) A role for actin in regulating apoptosis/programmed cell death: Evidence spanning yeast, plants and animals. *Biochem. J.* 413, 389–404.
- (83) Smertenko, A., and Franklin-Tong, V. E. (2011) Organisation and regulation of the cytoskeleton in plant programmed cell death. *Cell Death Differ.* 18, 1263–1270.
- (84) D'Angeli, S., Malho, R., and Altamura, M. M. (2003) Low-temperature sensing in olive tree: Calcium signalling and cold acclimation. *Plant Sci.* 165, 1303–1313.

## ■ NOTE ADDED AFTER ASAP PUBLICATION

This article was published ASAP on October 10, 2011. The second paragraph in the second column of the fourth page has been updated. The corrected version was posted on October 12, 2011.

## SUPPORTING INFORMATION

### **Phosphorylation of *Thellungiella salsuginea* dehydrins TsDHN-1 and TsDHN-2 facilitates cation-induced conformational changes and actin assembly**

Luna N. Rahman<sup>1</sup>,  
Graham S.T. Smith<sup>1</sup>,  
Vladimir V. Bamm<sup>1</sup>,  
Janine A.M. Voyer-Grant<sup>1</sup>,  
Barbara A. Moffatt<sup>2</sup>,  
John R. Dutcher<sup>3</sup>,  
George Harauz<sup>1\*</sup>.

<sup>1</sup>Department of Molecular and Cellular Biology,  
University of Guelph, Guelph, ON, N1G 2W1, Canada.

<sup>2</sup>Department of Biology,  
University of Waterloo, Waterloo, ON, N2L 3G1, Canada.

<sup>3</sup>Department of Physics,  
University of Guelph, Guelph, ON, N1G 2W1, Canada.

## SUPPORTING FIGURES

**Figure S1.** Sodium dodecyl sulphate polyacrylamide gel electrophoresis pattern of expression of SUMO-tagged TsDHN-1 (major band at roughly 70 kDa, predicted  $M_r$  30140.3 Da plus the  $M_r$  13035.6 Da of His<sub>6</sub>-SUMO), and TsDHN-2 (major band at roughly 45 kDa, predicted  $M_r$  21435.1 Da plus the  $M_r$  13035.6 Da of His<sub>6</sub>-SUMO). The abnormal migration of these dehydrins is characteristic of intrinsically disordered proteins [(1-4)], and is especially marked for TsDHN-1 due to its high net charge [(5;6)]. The molecular masses of the markers are indicated in kDa.

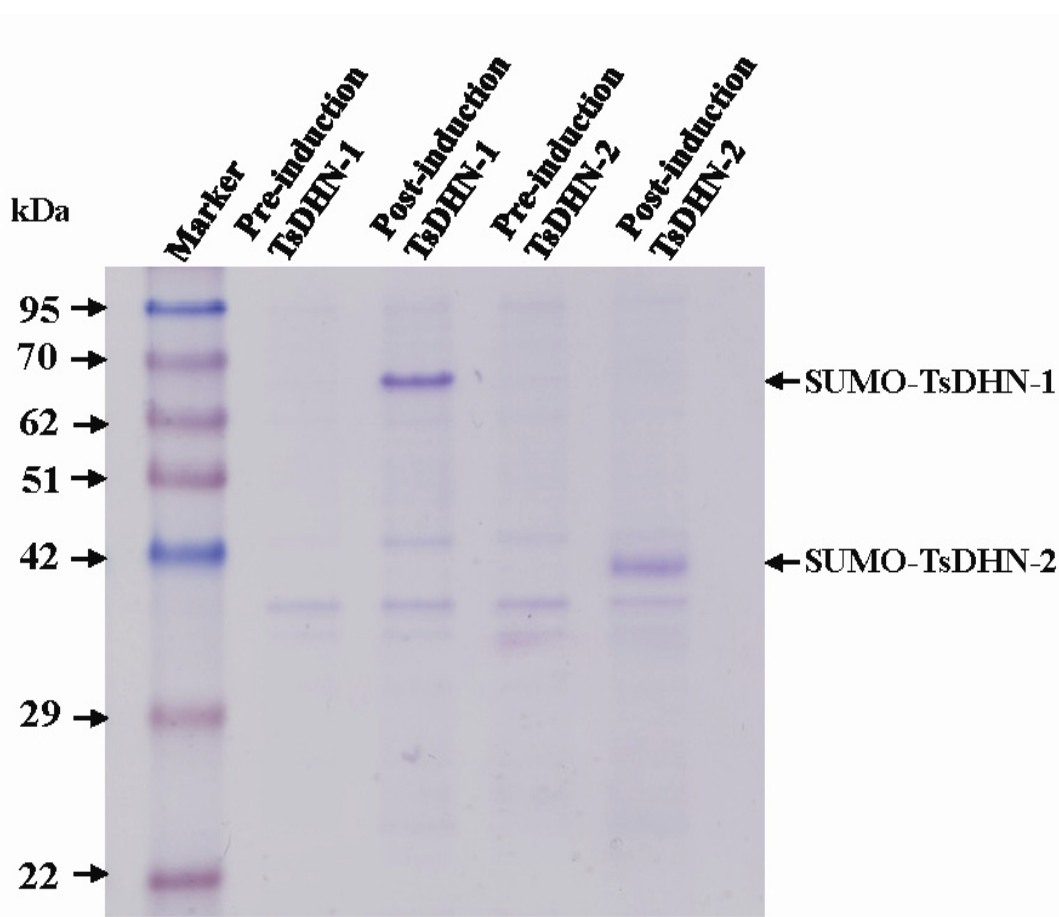


**Figure S2.** Mass spectra (ESI – electrospray ionization) for *in vitro* phosphorylated TsDHN-1 and TsDHN-2. Each phosphorylation event adds 80 Da of mass. Spectra indicate that the major proportion of TsDHN-1 ( $M_r = 30140.3$  kDa) is phosphorylated at two sites, and that the major proportion of TsDHN-2 ( $M_r = 21435.1$  Da) is phosphorylated at one site.

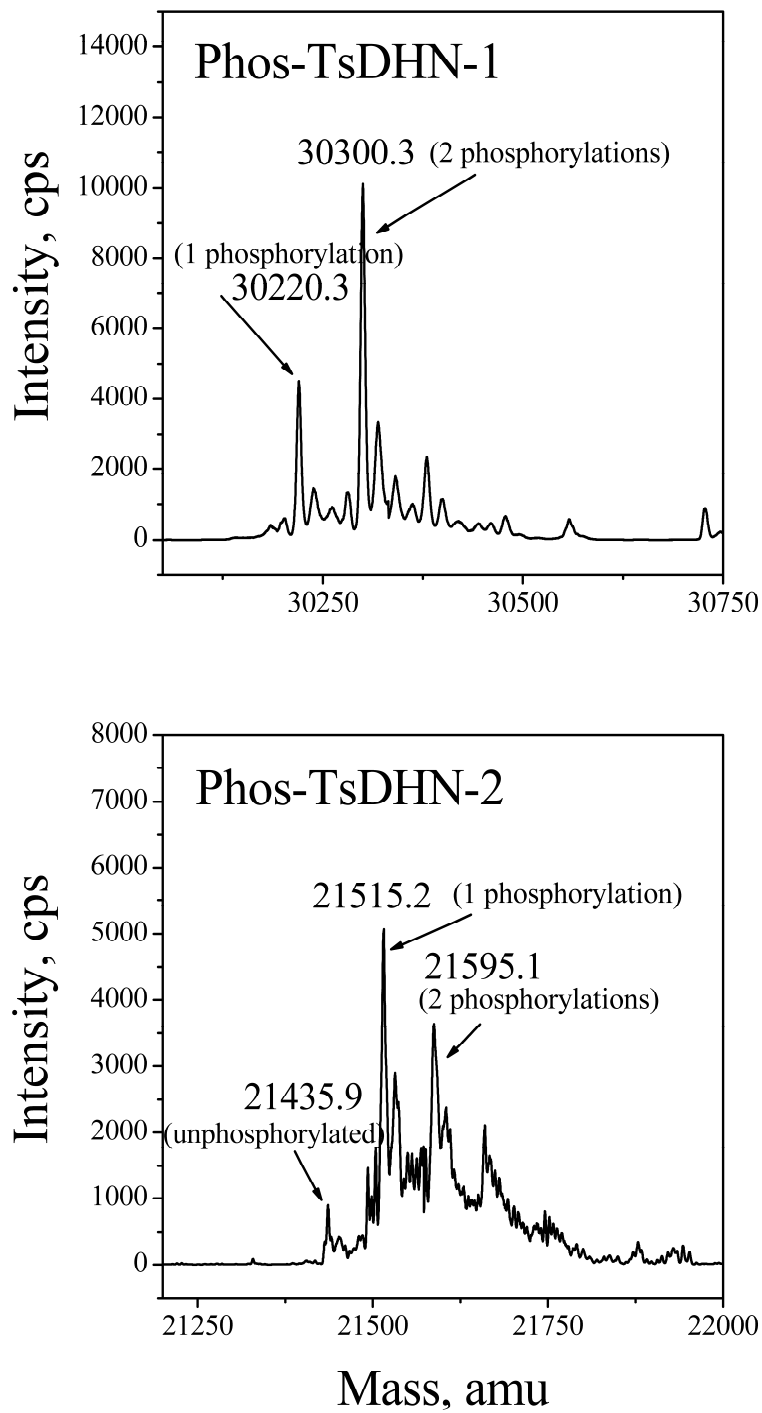
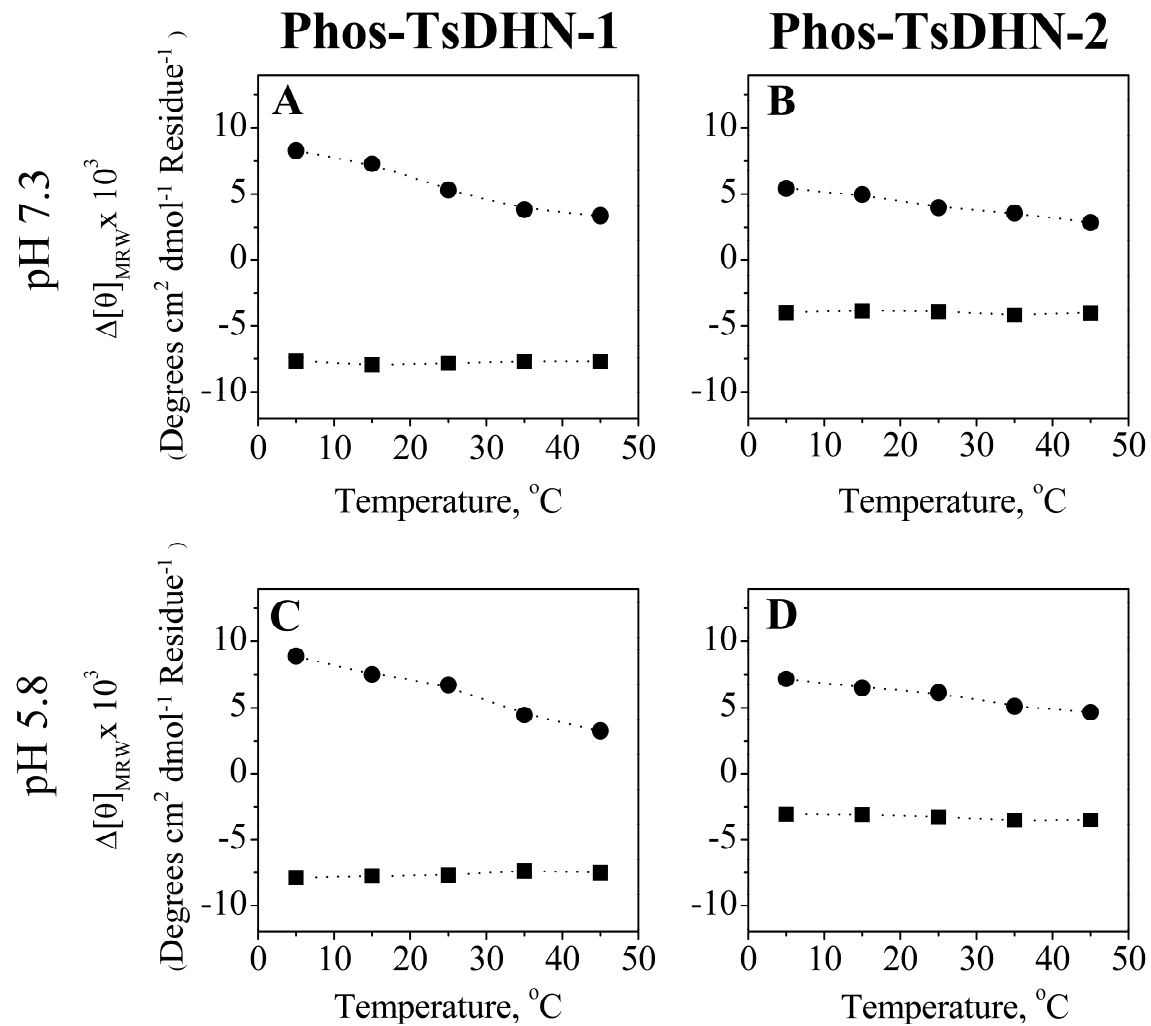


**Figure S3.** Molar ellipticity  $\theta$  at 208 nm (filled squares ■), and the differences of molar ellipticity  $\Delta[\theta]_{220-197}$  (filled circles ●), for phosphorylated TsDHN-1 and phosphorylated TsDHN-2 at variable temperatures, and at (A, B) pH 7.3 or (C, D) pH 5.8.



## SUPPORTING TABLES

**Table S1.** Effect of zinc on the secondary structure components of unphosphorylated and phosphorylated TsDHN-1 bound to large unilamellar vesicles mimicking the plant chloroplast membrane (MGDG:DGDG:SQDG:PC:DMPG:PE:PI at 51:26:7:3:9:1 by wt%), with a 1:10 molar ratio of [TsDHN-1]:[Zn<sup>2+</sup>]. The columns show the percentage area of each peak, with errors representing the standard deviation of three replicates of data sets. The values will not necessarily add up precisely to 100% because of rounding.

Components of TsDHN-1	$\lambda_{\max}$ , cm <sup>-1</sup>	Absence of Zn <sup>2+</sup>	Presence of Zn <sup>2+</sup>	Components of Phos-TsDHN-1	$\lambda_{\max}$ , cm <sup>-1</sup>	Absence of Zn <sup>2+</sup>	Presence of Zn <sup>2+</sup>
$\beta$ -strand	1627-28	20.0±1.5	23.9±0.5	$\beta$ -strand	1629	14.6±.4	13.1±2.2
Random coil	1642-45	40.9±1.2	31.1±0.2	Random coil	1643	19.7±1.4	18.9±2.5
$\alpha$ -helix	1659	14.1±1.2	9.7±0.3	$\alpha$ -helix	1651	35.8±2.2	34.7±3.4
Turn	1671-73	25.0±1.2	35.4±0.2	Turn	1663	22.5±1.2	24.8±4.0
				Anti-parallel $\beta$ -strand	1679	7.5±0.2	9.1±2.2
Total		100.0%	100.0%			100.0%	100.6%

**Table S2.** Effect of zinc on the secondary structure components of unphosphorylated and phosphorylated TsDHN-2 bound to large unilamellar vesicles mimicking the plant chloroplast membrane (MGDG:DGDG:SQDG:PC:DMPG:PE:PI at 51:26:7:3:9:1 by wt%), with a 1:10 molar ratio of [TsDHN]:[Zn<sup>2+</sup>]. The columns show the percentage area of each peak, with errors representing the standard deviation of three replicates of data sets. The values will not necessarily add up precisely to 100% because of rounding.

Components of TsDHN-2	$\lambda_{\max}$ , cm <sup>-1</sup>	Absence of Zn <sup>2+</sup>	Presence of Zn <sup>2+</sup>	Components of Phos-TsDHN-2	$\lambda_{\max}$ , cm <sup>-1</sup>	Absence of Zn <sup>2+</sup>	Presence of Zn <sup>2+</sup>
$\beta$ -strand	1629	19.1±0.8	17.7±2.6	$\beta$ -strand	1627	14.3±1.8	14.3±0.2
Random coil	1643	18.7±1.2	16.2±0.4	Random coil	1640	24.3±1.8	16.5±1.1
$\alpha$ -helix	1651	33.9±1.6	32.7±3.3	$\alpha$ -helix	1653	32.1±2.1	36.4±1.7
Turn	1663	21.4±1.8	24.9±2.5	Turn	1668	22.2±3.6	22.8±0.6
Anti-parallel $\beta$ -strand	1679	7.1±0.4	8.6±2.5	Anti-parallel $\beta$ -strand	1680	7.2±2.1	10.1±0.4
Total		100.0%	100.0%			100.0%	100.0%

**Table S3.** Effect of zinc on the secondary structure components of unphosphorylated and phosphorylated TsDHN-1 bound to large unilamellar vesicles mimicking the plant plasma membrane (PC:PE:PI at 33:47:20 by wt%), with a 1:10 molar ratio of [TsDHN]:[Zn<sup>2+</sup>]. The columns show the percentage area of each peak, with errors representing the standard deviation of three replicates of data sets. The values will not necessarily add up precisely to 100% because of rounding.

Components of TsDHN-1	$\lambda_{\max}$ , cm <sup>-1</sup>	Absence of Zn <sup>2+</sup>	Presence of Zn <sup>2+</sup>	Components of Phos-TsDHN-1	$\lambda_{\max}$ , cm <sup>-1</sup>	Absence of Zn <sup>2+</sup>	Presence of Zn <sup>2+</sup>
$\beta$ -strand	1625	18.9±0.2	26.2±0.3	$\beta$ -strand	1630	11.8±0.9	13.1±3.7
Random coil	1647	55.0±0.7	42.1±0.9	Random coil	1640	22.4±0.8	18.2±1.2
Turn	1672	26.1±0.6	31.7±0.5	$\alpha$ -helix	1653	36.6±0.6	36.9±3.8
				Turn	1670	16.5±2.4	21.8±0.7
				Anti-parallel $\beta$ -strand	1679	12.6±0.8	10.0±0.6
Total		100.0%	100.0%			100.0%	100.0%

**Table S4.** Effect of zinc on the secondary structure components of unphosphorylated and phosphorylated TsDHN-2 bound to large unilamellar vesicles mimicking the plant plasma membrane (PC:PE:PI at 33:47:20 by wt%), with a 1:10 molar ratio of [TsDHN]:[Zn<sup>2+</sup>]. The columns show the percentage area of each peak, with errors representing the standard deviation of three replicates of data sets. The values will not necessarily add up precisely to 100% because of rounding.

Components of TsDHN-2	$\lambda_{\max}$ , cm <sup>-1</sup>	Absence of Zn <sup>2+</sup>	Presence of Zn <sup>2+</sup>	Components of Phos-TsDHN-2	$\lambda_{\max}$ , cm <sup>-1</sup>	Absence of Zn <sup>2+</sup>	Presence of Zn <sup>2+</sup>
$\beta$ -strand	1627	19.6±1.8	17.2±3.9	$\beta$ -strand	1630	15.2±0.4	14.8±0.8
Random coil	1644	20.4±0.1	17.4±1.3	Random coil	1640	23.8±0.3	19.4±0.5
$\alpha$ -helix	1658	33.5±0.6	35.1±3.5	$\alpha$ -helix	1653	33.4±0.2	31.2±0
Turn	1671	15.0±2.3	20.9±0.6	Turn	1670	21.6±0.1	24.0±1.2
Anti-parallel $\beta$ -strand	1684	11.5±0.6	9.5±0.6	Anti-parallel $\beta$ -strand	1679	6.2±0.2	10.9±1.5
Total		100.0%	100.0%			100.0%	100.1%

## SUPPORTING REFERENCES

1. Armstrong, D. J. and Roman, A. (1993) The anomalous electrophoretic behavior of the human papillomavirus type 16 E7 protein is due to the high content of acidic amino acid residues. *Biochem. Biophys. Res. Commun.* 192, 1380-1387.
2. Bates, I. R., Matharu, P., Ishiyama, N., Rochon, D., Wood, D. D., Polverini, E., Moscarello, M. A., Viner, N. J., and Harauz, G. (2000) Characterization of a recombinant murine 18.5-kDa myelin basic protein. *Protein Expr. Purif.* 20, 285-299.
3. Iakoucheva, L. M., Kimzey, A. L., Masselon, C. D., Smith, R. D., Dunker, A. K., and Ackerman, E. J. (2001) Aberrant mobility phenomena of the DNA repair protein XPA. *Protein Sci.* 10, 1353-1362.
4. Receveur-Bréchot, V., Bourhis, J. M., Uversky, V. N., Canard, B., and Longhi, S. (2006) Assessing protein disorder and induced folding. *Proteins* 62, 24-45.
5. Rahman, L. N., Chen, L., Nazim, S., Bamm, V. V., Yaish, M. W., Moffatt, B. A., Dutcher, J. R., and Harauz, G. (2010) Interactions of intrinsically disordered *Thellungiella salsuginea* dehydrins TsDHN-1 and TsDHN-2 with membranes - synergistic effects of lipid composition and temperature on secondary structure. *Biochem. Cell Biol.* 88, 791-807.
6. Rahman, L. N., Bamm, V. V., Voyer, J. A. M., Smith, G. S., Chen, L., Yaish, M. W., Moffatt, B. A., Dutcher, J. R., and Harauz, G. (2011) Zinc induces disorder-to-order transitions in free and membrane-associated *Thellungiella salsuginea* dehydrins TsDHN-1 and TsDHN-2: a solution CD and solid-state ATR-FTIR study. *Amino Acids* 40, 1485-1502.